

Inter-model comparison of global hydroxyl radical (OH) distributions and their impact on atmospheric methane over the 2000-2016 period

Yuanhong Zhao¹, Marielle Saunois¹, Philippe Bousquet¹, Xin Lin^{1*}, Michaela I. Hegglin², Josep G. Canadell³, Robert B. Jackson⁴, Didier A. Hauglustaine¹, Sophie Szopa¹, Ann R. Stavert⁵, Nathan Luke Abraham^{6, 7}, Alex T. Archibald^{6, 7}, Slimane Bekki⁸, Makoto Deushi⁹, Patrick Jöckel¹⁰, B éatrice Josse¹¹, Douglas Kinnison¹², Ole Kirner¹³, Virginie Mar écal¹¹, Fiona M. O'Connor¹⁴, David A. Plummer¹⁵, Laura E. Revell^{16, 17}, Eugene Rozanov^{16, 18}, Andrea Stenke¹⁶, Sarah Strode^{19, 20}, Simone Tilmes²¹, Edward J. Dlugokencky²², and Bo Zheng¹

10

¹ Laboratoire des Sciences du Climat et de l'Environnement, LSCE-IPSL (CEA-CNRS-UVSQ), Université Paris-Saclay, 91191 Gif-sur-Yvette, France

² Department of Meteorology, University of Reading, Earley Gate, Reading RG6 6BB, United Kingdom

³ Global Carbon Project, CSIRO Oceans and Atmosphere, Canberra, Australian Capital Territory 2601, Australia

15

⁴ Earth System Science Department, Woods Institute for the Environment, and Precourt Institute for Energy, Stanford University, Stanford, CA 94305, USA

⁵ CSIRO Oceans and Atmosphere, Aspendale, Victoria, 3195, Australia

⁶ Department of Chemistry, University of Cambridge, CB2 1EW, UK

20 ⁷ NCAS-Climate, University of Cambridge, CB2 1EW, UK

⁸ LATMOS, Université Pierre et Marie Curie, 4 Place Jussieu Tour 45, couloir 45-46, 3^e étage Boite 102, 75252, Paris Cedex 05, France

⁹ Meteorological Research Institute, 1-1 Nagamine, Tsukuba, Ibaraki, 305-0052, Japan

¹⁰ Deutsches Zentrum für Luft- und Raumfahrt (DLR), Institut für Physik der Atmosphäre, Oberpfaffenhofen, Germany

25

¹¹Centre National de Recherches Météorologiques, Université de Toulouse, Météo-France, CNRS, Toulouse, France

¹²Atmospheric Chemistry Observations and Modeling Laboratory, National Center for Atmospheric Research, 3090 Center Green Drive, Boulder, CO, 80301, USA

30 ¹³ Steinbuch Centre for Computing, Karlsruhe Institute of Technology, Karlsruhe, Germany

¹⁴ Met Office Hadley Centre, Exeter, EX1 3PB, UK

¹⁵ Climate Research Branch, Environment and Climate Change Canada, Montréal, Canada

¹⁶ Institute for Atmospheric and Climate Science, ETH Zürich (ETHZ), Zürich, Switzerland

¹⁷ School of Physical and Chemical Sciences, University of Canterbury, Christchurch, New Zealand

35 ¹⁸ Physikalisch-Meteorologisches Observatorium Davos World Radiation Centre, Dorfstrasse 33, 7260 Davos Dorf

¹⁹ NASA Goddard Space Flight Center, Greenbelt, MD, USA

²⁰ Universities Space Research Association (USRA), GESTAR, Columbia, MD, USA

²¹ National Center for Atmospheric Research, Boulder, CO, USA

40 ²² Global Monitoring Division, NOAA Earth System Research Laboratory, Boulder, CO, USA

* Now at: Climate and Space Sciences and Engineering, University of Michigan, Ann Arbor, MI 48109, USA

45 *Correspondence to:* Yuanhong Zhao (yuanhong.zhao@lsce.ipsl.fr)

Abstract

The modeling study presented here aims to estimate how uncertainties in global hydroxyl radical (OH) distributions, variability, and trends may contribute to resolve discrepancies between simulated and observed methane (CH₄) changes since 2000. A multi-model ensemble of 14 OH fields were analysed and were aggregated into 64 scenarios to force the offline atmospheric chemistry transport model LMDz with a standard CH₄ emission scenario over the period 2000-2016. The multi-model simulated global volume-weighted tropospheric mean OH concentration([OH]) averaged over 2000-2010 ranges between 8.7×10^5 and 12.8×10^5 molec cm⁻³. The inter-model differences in tropospheric OH burden and vertical distributions are mainly determined by the differences in the nitrogen oxide (NO) distributions, while the spatial discrepancies between OH fields are mostly due to differences in natural emissions and VOC chemistry. From 2000 to 2010, most simulated OH fields show an increase of $0.1-0.3 \times 10^5$ molec cm⁻³ in the tropospheric mean [OH], with year-to-year variations much smaller than during the historical period 1960-2000. Once ingested into the LMDz model, these OH changes translated into a 5 to 15 ppbv reduction in CH₄ mixing ratio in 2010, which represent 7%-20% of the model simulated CH₄ increase due to surface emissions. Between 2010 and 2016, the ensemble of simulations showed that OH changes could lead to a CH₄ mixing ratio uncertainty of $> \pm 30$ ppbv. Over the full 2000-2016 time period, using a common state-of-the-art but non-optimized emission scenario, the impact of [OH] changes tested here can explain up to 54% of the gap between model simulations and observations. This result emphasizes the importance of better representing OH abundance and variations in CH₄ forward simulations and emission optimizations performed by atmospheric inversions.

1 Introduction

70 The hydroxyl radical (OH) is the main oxidizing agent in the troposphere (Levy, 1971). OH is produced by the reaction of water vapor with excited oxygen atoms ($O(^1D)$), produced by ozone (O_3) photolysis ($\lambda < 340\text{nm}$). In the troposphere, OH is rapidly removed by reactions with carbon monoxide (CO), methane (CH_4) and non-methane volatile organic compounds (NMVOCs) to generate hydroperoxyl radical (HO_2) or organic peroxy radicals (RO_2), resulting in a short lifetime of a few seconds (Logan et al., 1981; 75 Lelieveld et al., 2004). HO_2 and RO_2 can further react with nitrogen oxide (NO) to regenerate OH (Crutzen, 1973; Zimmerman et al., 1987). At high latitudes, such a secondary production plays an important role, because the OH primary production is limited by the supply of $O(^1D)$ and water vapor (Spivakovsky et al., 2000). The abundance of OH reflects the combined effects of atmospheric composition (tropospheric O_3 , and NO, CO, CH_4 , and NMVOCs) and of meteorological factors such as humidity, UV radiation, and 80 temperature.

Due to its short lifetime, global [OH] is difficult to estimate from direct measurements. Current understanding on global [OH] has been obtained either from inversion of 1-1-1trichloroethane (methyl chloroform, MCF) (Prinn et al., 2005; Bousquet et al., 2005; Montzka et al., 2011; Rigby et al., 2017; 85 Turner et al., 2017), or using atmospheric chemistry models (Naik et al., 2013; Voulgarakis et al., 2013, Lelieveld et al., 2016). The former approach relies on the fact that OH is the main sink of MCF and on the hypotheses that emissions and concentrations of MCF are well known and well measured, respectively. The latter approach relies on chemistry-transport modeling with chemistry schemes of varying complexity. The global mass-weighted tropospheric mean [OH] in the 2000s calculated by atmospheric chemistry 90 models was found to be about $11.5 \times 10^5 \text{ molec cm}^{-3}$, with an inter-model dispersion of $\pm 15\%$ (Naik et al., 2013; Voulgarakis et al., 2013). Atmospheric chemistry models usually calculate higher [OH] over the Northern hemisphere than the Southern hemisphere (N/S ratio > 1) (Naik et al., 2013) whereas MCF and ^{14}C observations indicate a N/S ratio slightly smaller than 1 (Brenninkmeijer et al., 1992; Bousquet et

al., 2005; Patra et al., 2014).

95

OH determines the lifetime of most pollutants and non-CO₂ greenhouse gases including CH₄, the second most important anthropogenic greenhouse gas after carbon dioxide (CO₂) (Ciais et al., 2013). About 90% of tropospheric CH₄ is removed by reacting with OH (Ehhalt et al., 1974; Kirschke et al., 2013; Saunio et al., 2016). The tropospheric CH₄ chemical lifetime against OH oxidation (global annual mean atmospheric CH₄ burden divided by annual CH₄ tropospheric loss by OH) calculated by the models that participated in the Atmospheric Chemistry and Climate Model Inter-comparison Project (ACCMIP) is 9.3±1.6 years, and the CH₄ total lifetime including all sink processes is 8.3±0.8 years (Naik et al., 2013; Voulgarakis et al., 2013), smaller than that of 9.1±0.9 years lifetime constrained by observations (Prather et al., 2012).

105

The tropospheric CH₄ burden has more than doubled compared to the pre-industrial era due to anthropogenic activities and climate change, resulting in about 0.62 W m⁻² additional radiative forcing (Etminan et al., 2016). The global mean CH₄ growth rate decreased to near zero in the early 2000s but resumed increasing at ~5ppbv yr⁻¹ since 2006 and reached more than 10 ppbv yr⁻¹ in 2014 and in 2018 (Ed Dlugokencky, NOAA/ESRL, 2019). The growth rate of CH₄ is determined by the imbalance of its sources, primarily from anthropogenic activities (agriculture, waste, fossil fuel production and usage, and biomass burning) but also from natural emissions (mainly wetland and other inland waters), and sinks (OH oxidation, other chemical reactions with chlorine and oxygen radicals, and soil uptake). The precise reasons for the stagnation and renewed CH₄ growths still remains unclear (e.g. Rigby et al 2017; Saunio et al., 2017; Nisbet et al., 2019).

115

Several studies have linked such CH₄ variations to inter-annual variations and trend of OH. Based on MCF inversions, McNorton et al. (2016) concluded that an increase in [OH] significantly contributed to

the stable atmospheric CH₄ before 2007; Rigby et al. (2008) found that a decrease of $4 \pm 14\%$ in [OH] could partly explain the CH₄ growth between 2006 and 2007; Bousquet et al. (2011) found a smaller decrease in [OH] (<1% over the two years) and attributed the increase in CH₄ mostly to enhanced emissions over tropical regions; Montzka et al. (2011) also calculated a small inter-annual variation of $2.3 \pm 1.5\%$ in [OH] during 1998 to 2007. More recently, based on multi-species box model inversions, Rigby et al. (2017) and Turner et al. (2017) inferred a decrease of $8 \pm 11\%$ and 7% in [OH] during 2004-2014 and 2003-2016 respectively. Both of these studies suggested that such a decrease in [OH] is equivalent to an increase of more than 20 Tg yr⁻¹ in CH₄ emissions, and therefore could significantly contribute to explain the post-2007 CH₄ atmospheric growth, although a solution with constant OH cannot be discarded. Meanwhile, not only the OH trend calculated by atmospheric chemistry models cannot reach consensus, but it can also be different from the OH trend inferred by top-down approaches from observations. Indeed, Dalsøren et al. (2016) simulated ~ 8% increase in OH during 1970 to 2012, while other models mostly calculated only a small increase of [OH] (decrease in CH₄ lifetime) or no trend in [OH] from 1980s to 2000s (e.g. Voulgarakis et al., 2013; Nicely et al., 2018). Top-down observation-constrained approaches (e.g. Rigby et al., 2017) tend to find flat to decreasing OH trend over this period but with larger year-to-year variations than models. The discrepancy between individual process-based models and MCF-proxy approaches, and the uncertainties, limit our ability to be conclusive on the role of [OH] changes to explain the CH₄ changes over the past decades.

To better understand OH distributions, trends, and influences on CH₄ since 2000, we have performed an inter-model comparison of 14 OH fields, including 11 derived from chemistry transport and chemistry-climate models that took part in the phase 1 of the Chemistry-Climate Model Initiative (CCMI) (Hegglin and Lamarque, 2015; Morgenstern et al., 2017), 2 from different configurations of the LSCE atmospheric chemistry transport model LMDz-INCA (Hauglustaine et al., 2004; Szopa et al., 2013), and 1 from the TRANSCOM 2011 inter-comparison exercise (Patra et al., 2011). We then conducted an ensemble of CH₄

simulations with different OH fields using the LMDz chemistry-transport model to estimate a range for
145 the contribution of changes in [OH] to the atmospheric CH₄ mixing ratio changes since 2000, and to relate
this contribution to spatio-temporal characteristics of the different OH fields. Year-to-year integrations of
CCMI and INCA models driven by time-varying emissions and meteorology facilitate the investigation
of interannual variability in OH, which was not possible using the ACCMIP time-slice simulations. In the
following, our analysis first provides a brief description of the OH fields used in this study and the LMDz
150 offline model (section 2). Section 3 compares the OH fields, analyses the factors contributing to inter-
model differences and presents their inter-annual variability. Section 4 presents and discusses the impact
of the different OH fields on the global CH₄ burden and growth rates simulated by LMDz. Section 5
summarizes the results and conclusion.

155 **2 Method**

2.1 OH fields

The CCMI project aims to conduct a detailed evaluation of atmospheric chemistry models in order to
assess uncertainties in the models' projections of various climate-related topics such as tropospheric
160 composition (Hegglin and Lamarque, 2015; Morgenstern et al., 2017). The CCMI OH fields used in our
study are obtained from 10 different models and 3 CCMI reference experiments: REF-C1 (covering the
time period 1960-2010), REF-C2 (covering 1960-2100), and REF-C1SD (1980-2010). The REF-C1
experiment is driven by state-of-the-art historical forcings and sea surface temperatures (sst) and sea ice
concentrations (sic) based on observations, while the REF-C2 experiment is using either coupled ocean
165 and sea ice modules or prescribes sst and sic obtained from another climate model. Since the REF-C1
experiment is supposed to be more realistic regarding sea surface conditions, our analysis focused on OH
fields from the REF-C1 experiment before 2010 and only tested the influences of OH on CH₄ simulations
after 2010 by applying the inter-annual variability from the REF-C2 experiment. The models of REF-

C1SD experiment are nudged towards reanalysis datasets. The REF-C1SD experiment is not analyzed in
170 the main text since it has been conducted by only part of the models and covers a shorter time period. A
comparison of spatial and vertical distributions of OH fields from REF-C1 experiment with that from
REF-C1SD reveals only small latitudinal differences (<10%, see Section S1). Detailed descriptions of
CCMI simulations can be found in Morgenstern et al. (2017).

175 In this study, we used only the CCMI models that include detailed tropospheric ozone chemistry as listed
in Table 1. Note that EMAC offers fields at two different model resolutions. The level of detail in chemical
mechanism, in particular with respect to included NMVOCs, varies among the models. For example,
CMAM does not include any NMVOC species, but added 250 Tg CO emissions to account for CO
production from isoprene oxidation. UМУKCA-UCAM only include HCHO (formaldehyde) and
180 SOCOL3 only include HCHO and C₅H₈ (isoprene). Other models include multiple primary NMVOC
species and more complex VOC chemistry.

The anthropogenic emissions recommended for the two CCMI reference simulations are the MACCity
inventory (Granier et al., 2011) for 1960-2000. After 2000, the REF-C1 experiment continued to use the
185 MACCity inventory (which follow the RCP8.5 inventory after 2000), while the REF-C2 used the RCP6.0
inventory (Masui et al., 2011). The CMAM model did not follow this procedure and used the ACCMIP
historical database of emissions (Lamarque et al., 2010) until 2000 followed by RCP8.5 emissions (Riahi
et al., 2011) instead. Biomass burning emissions used in REF-C1 are RETRO inventory (Schultz et al.
2008) before 1996 and GFEDv3 inventory (van der Werf et al., 2010) for 1997-2010 with interannual
190 variability. CCMI model simulations also include natural emissions from lightning, soil and biogenic
sources. Lightning NO_x emissions are calculated based on meteorological data such as cloud top height
(Price and Rind, 1994; Grewe et al., 2001) and updraft mass flux (Allen and Pickering, 2002). Soil NO_x
emissions are calculated interactively in EMAC and GEOSCCM using the scheme described by Yienger

and Levy (1995), but are prescribed in other models. Biogenic NMVOC emissions in CESM and
195 GEOSCCM are calculated based on the distribution of plant functional types and meteorology conditions
with MEGAN, whereas the other models apply prescribed biogenic NMVOC emissions.

The CCMi models do not represent CH₄ emissions explicitly but prescribe CH₄ surface mixing ratios vary
in time according to the RCP6.0 scenario (global mean of ~1750ppbv averaged over 2000-2010) with
200 different spatial distributions: GEOSCCM, CESM and EMAC models consider the full latitudinal
gradient and prescribe CH₄ surface mixing ratios about 50 ppbv higher over the Northern hemisphere
than over the Southern hemisphere; while CMAM, MRI-ESM1r1, and SOCOL3 use global uniform
values. Photolysis rates are calculated either following online schemes such as FAST-JX (Neu et al., 2007;
Telford et al., 2013) by GEOSCCM, HadGEM3-EA, UMUKA-UCAM, JVAL (Sander et al., 2014) by
205 EMAC, or based on look-up tables with online cloud corrections by the rest of the models used in this
study. Kinetics and photolysis data are mainly from Sander et al. (2011) with a few exceptions. More
information on model characteristics can be found in Morgenstern et al. (2017) and references listed in
Table 1.

210 Additionally to CCMi OH fields, we also included 2 OH fields simulated by the Interaction with
Chemistry and Aerosols (INCA) coupled to the general circulation model of the Laboratoire de
Météorologie Dynamique (LMD), LMDz (Sadourny and Laval, 1984; Hourdin and Armengaud, 1999;
Hourdin et al., 2006; Hauglustaine et al., 2004). The two INCA simulations are driven by different
versions of the LMDz GCM (INCA NMHC-AER-S covering time period 2000-2010 (Terrenoire et al.,
215 2019), and INCA NMHC covering time period 2000-2009 (Szopa et al., 2013)), which provide different
water vapor fields, and include different chemistry and emissions. The INCA NMHC-AER-S used the
latest version of INCA model including both gas phase (NMHC) and aerosol (AER) chemistry in the
troposphere and the stratosphere (S) (Terrenoire et al., 2019), while INCA NMHC used a former version

that only includes tropospheric gas-phase chemistry (Szopa et al., 2013). Anthropogenic emissions from
220 Short-Lived Pollutants (ECLIPSE) inventory (Stohl et al., 2015) for 2005 and RCP 85 emission inventory
(Riahi et al., 2011)) for 2010 are applied to every year of INCA NMHC-AER-S and INCA NMHC
simulations, respectively.

Finally, we included in this study the OH field used in TransCom simulations, which results from a
225 combination of the semi-empirical tropospheric 3-dimensional OH field from Spivakovsky et al. (2000)
and a 2-dimensional simulated stratospheric OH for year 2000. The tropospheric OH was calculated using
prescribed chemical species (O_3 , nitrogen oxides, and CO) as well as meteorological fields (temperature,
humidity, and cloud optical depth) to fit the observations. The original tropospheric [OH] has been
reduced by 8% to match CH_3CCl_3 observations (Patra et al., 2011). The TransCom OH field is only
230 climatological (one year of monthly fields).

In total, we compared 14 OH fields: 11 from CCMI, 2 from the online LMDz-INCA model and 1 from
TransCom. We analyzed spatial distributions and annual variations of OH fields by calculating volume-
weighted tropospheric mean [OH] with tropopause pressure using WMO tropopause definition on 3D
235 temperature for each model (World Meteorological Organization, 1957). Since employing different
weightings can result in large differences in mean [OH] (Lawrence et al., 2001), we also calculated dry
air mass-weighted tropospheric mean [OH] to better compare with previous studies.

2.2 LMDz model simulations

240 2.2.1 Model description and setup

We have run the offline version LMDz5B of the LMDz model (Locatelli et al., 2015) at a horizontal
resolution of $3.75^\circ \times 1.85^\circ$ with 39 vertical layers up to 3 hPa to assess the impact of OH on tropospheric
CH₄. All monthly mean OH fields have been interpolated to the LMDz model grid. The transport of

atmospheric tracers is driven by prescribed air mass fluxes provided by the general circulation model
245 LMDz with horizontal wind fields nudged to ERA-Interim re-analysis meteorology data produced by the
European Center for Medium-Range Weather Forecasts (Dee et al, 2011). The vertical transport is
parameterized according to updates of the Emanuel (1991) scheme for convection and of the Louis (1979)
scheme for boundary layer mixing (Hourdin et al., 2016; Locatelli et al., 2015). Chemistry module applied
here is the simplified chemistry module SACS (Pison et al., 2009). Chemical sinks of CH₄ are calculated
250 using prescribed three-dimensional OH and O(¹D) fields, and variation in CH₄ cannot feedback on OH.
No chlorine-related sink is simulated in this version of the model. To assess the influences of OH only,
all LMDz simulations used the same O(¹D) fields generated by INCA model simulations. The reaction rate
co-efficient (k) for CH₄ destruction by OH in the model is computed depending on temperature following
Sander et al. (2011):

$$255 \quad k = 2.45 \times 10^{-12} e^{-1775 \times (\frac{1}{T})} \quad (1)$$

The LMDz model has been applied in various studies focusing on long-lived gases such as CH₄, CO₂ and
MCF (Bousquet et al., 2005; Pison et al., 2009; Lin et al., 2018). It has also been used in model inter-
comparison projects such as the TransCom experiment (Patra et al., 2011) with the simplified chemistry
module SACS (Pison et al., 2009) and CCMI (Morgenstern et al., 2017) but only with the stratospheric
260 chemistry model PEPROBUS (Jourdain et al., 2008).

The CH₄ emissions input to LMDz simulations are provided by the Global Carbon Project (GCP) methane
and include anthropogenic and biofuel emissions from EDGARv4.3.2 (Janssens-Maenhout et al., 2017),
the mean wetland emissions from Poulter et al., (2017), fire emissions from the Global Fire Emissions
265 Database Version 4.1 (GFED4) (Randerson et al., 2018), termite emissions as described by Saunois et al.
(2016), geological emissions based on the spatial distribution of Etiope (2015), ocean emissions from
Lambert and Schmidt (1993) and soil uptake from Ridgwell et al. (1999). EDGARv4.3.2 data, available

until 2012, were extrapolated from 2013 to 2016 using economical statistics according to the methodology described by Saunio et al., (2016). Anthropogenic and fire emissions vary from 2000 to 2016 while
270 natural emissions are applied as a climatology.

The spatial distributions and annual variations of the CH₄ emissions during the study period are shown in Fig.1. CH₄ emissions range from 10 to 40 kg ha⁻¹ yr⁻¹ over most natural ecosystems and can exceed 100 kg ha⁻¹ yr⁻¹ over wetlands in Canada, South America, and Central Africa, as well as over densely
275 populated regions such as South and East Asia. Global net CH₄ emissions (soil uptake included) increased by 15% from 482 Tg yr⁻¹ in 2000 to 552 Tg yr⁻¹ in 2016. Of this 70 Tg yr⁻¹ increase, 60 Tg yr⁻¹ (85%) are emissions from the Northern hemisphere, mainly contributed by livestock (18 Tg yr⁻¹, 25%), oil and gas (16 Tg yr⁻¹, 23%), coal burning (17 Tg yr⁻¹, 24%) and waste (13Tg yr⁻¹, 18%). The three emission peaks in 2002, 2006 and 2015 are driven by biomass burning. This CH₄ emission scenario is state-of-the-art but
280 has not been optimized for the simulated CH₄ mixing ratios to fit the observations.

2.2.2 Model simulations

Two sets of experiments (steady-state and transient simulations) have been performed to examine the impacts of the input OH fields on the global CH₄ burden as well as the CH₄ spatial distribution and annual
285 variation. These tests excluded the OH fields from CESM1-CAM4chem and EMAC-L47MA, since they are similar to those of CESM1-WACCM and EMAC-L90MA, respectively. We also discarded the OH fields from HadGEM3-ES and UMUKCA-UCAM because output from these two models has been supplied on too coarse vertical pressure levels. Finally, 10 different OH fields (seven from CCMI, two from LMDz-INCA and one from Transcom) were used in the two sets of simulations.

290

Initially, for each OH field described in Sect. 3, we ran 30 consecutive years of LMDz simulations (with recycled same emissions, sinks, and meteorology of the year 2000) to allow the simulation to reach a

steady-state (CH_4 has an approximate lifetime of 9 years in the atmosphere). This step aims to examine the impact of the magnitude and distribution of OH on the global CH_4 burden.

295

Secondly, we performed transient simulations starting from the year 2000, which are forced by time-varying OH fields as well as time-varying emissions and meteorology fields. In order to compare the impacts of the different OH fields on realistic CH_4 mixing ratios, for each simulation (except the one using the OH fields from INCA NMHC), the OH field has been scaled to get the same LMDz simulated CH_4 loss as the one calculated by INCA NMHC in 2000, as INCA is the OH field consistently obtained using the LMDz transport. Then a series of LMDz model simulations is conducted to investigate the impact of the various OH fields on CH_4 growth rates between 2000 and 2016 as summarized in Table 2.

300

The standard simulations (Run_standard in Table 2) using the 10 different OH fields (7 are from CCM1 REF-C1), included annual variations and were performed from 2000 to 2010. Since REF-C1 experiments are only available up to 2010, the influence of OH on CH_4 mixing ratios after 2010 have been tested based on alternative scenarios. First, for CCM1 simulations, we tested a scenario that takes into account the annual variability from the REF-C2 experiments (Run_REF-C2 in Table 2). Previous ACCMIP model experiments showed slightly decreasing or increasing [OH] from 2000 to 2030 according to the largest or lowest radiative forcing pathways (RCP8.5 or RCP2.6), respectively (Voulgarakis et al., 2013). Top-down approaches suggested that global OH decreased by 0.5-1% annually from 2003 to 2016 (Rigby et al., 2017; Turner et al., 2017). In order to assess the recent change in [OH], we tested two additional scenarios between 2010 and 2016: one with [OH] increase of $+0.1\% \text{ yr}^{-1}$ (Run_OH_inc) according to the slightly changing of OH calculated by ACCMIP models and one with [OH] decrease of $-1\% \text{ yr}^{-1}$ (Run_OH_dec) according to obviously decreasing of OH calculated by top-down approaches constrained by observations. To assess influences from OH alone, we also conducted additional simulations of the period 2000 to 2016 with annually repeated prescribed [OH] equal to the year 2000 (Run_fix_OH) for each OH field. The

310

315

differences between these constant OH simulations and the corresponding time-varying OH simulations indicate the impact of OH inter-annual variations and trends on atmospheric CH₄ changes. In addition, we conducted two simulations during 2000-2010 driven by emission inventories fixed to the year 2000 to test the influences of the emission bias on our results. The two simulations use OH fields simulated by CESM-WACCM, one with inter-annual variations of OH (Run_fix_emis) and the other one with OH field fixed to 2000 (Run_fix_emis_OH).

3 Analysis of OH fields

3.1 Spatial distributions of tropospheric OH

Fig. 2 shows the spatial distributions of volume-weighted tropospheric mean [OH] averaged from 2000 to 2010. Based on the 14 OH fields we have assembled, the global mean volume-weighted tropospheric [OH] vary from 8.7×10^5 to 12.8×10^5 molec cm⁻³. SOCOL, which overestimation of [OH] have been reported by Staehelin et al. (2017), simulated the highest [OH]. To better compare with previous studies, we also calculated dry air mass-weighted tropospheric mean [OH] in table 4, which vary from 9.4×10^5 to 14.4×10^5 molec cm⁻³ and multi-model mean value of $11.3 \pm 1.3 \times 10^5$ molec cm⁻³. The tropospheric chemical CH₄ lifetime of the models that provided CH₄ chemical loss data are 8.7 ± 1.1 yr. Both the multi-model mean and the (large) range of [OH] as well as tropospheric CH₄ chemical lifetime are consistent with previous multi-model results given by the ACCMIP project (Naik et al., 2013; Voulgarakis et al., 2013), as well as with inversions based on MCF observations (Bousquet et al., 2005; Rigby et al., 2017). The model spread remains large as ~50% of the minimum value, as noted in previous studies (e.g. Naik et al., 2013).

Table 3 summarizes their inter-hemispheric ratios of tropospheric OH and mean values over four latitudinal bands. The inter-hemispheric ratios (N/S ratios) of CCMI and INCA OH fields are within the range of 1.2-1.5, similar to those from the ACCMIP project (Naik et al., 2013). In contrast, the TransCom

OH field has a ratio of 1.0, which is more consistent with that of MCF and ^{14}C constrained OH
345 (Brenninkmeijer et al., 1992; Krol and Lelieveld, 2003; Bousquet et al., 2005). However, as discussed by
Spivakovsky et al. (2000), the TransCom OH field may overestimate Southern Extra-tropics OH by ~25%.
The lower N/S ratios inferred from MCF observations are mainly due to high [OH] over the Southern
Tropics (35% higher than Northern Tropics) (Bousquet et al., 2005). In contrast, process-based simulated
OH is 10-26% more abundant over the Northern Tropics than over the Southern Tropics, and 35% to >
350 90% higher over 30°N-90°N than 30°S-90°S in the CCMI models. Previous studies have attributed the
inconsistency between the simulated and the observed OH N/S ratios to a model overestimation of O_3 and
underestimation of CO over the Northern Hemisphere (Naik et al., 2013; Young et al., 2013; Strode et al.,
2015), which also have been reported for CCMI models (Strode et al., 2016; Revell et al., 2018), as well
as to a lack of OH recycling due to the presence of VOCs over rainforest (mainly located in the Southern
355 Tropics) (Lelieveld et al., 2008; Archibald et al., 2011).

We further assessed the simulated OH spread by comparing the detailed spatial distributions of OH fields
in Fig. 2 and Fig.S2. Nearly all CCMI models and two versions of the INCA model simulated high [OH]
over eastern North American and South and East Asia, which is related to higher tropospheric O_3
360 concentrations (Cooper et al., 2014; Lu et al., 2018) and NO_x emissions from human activities (Lamarque
et al., 2010; Miyazaki et al., 2012). High [OH] over these emission hotspots dominate the aforementioned
simulated large N/S ratio. Some models also simulated high OH values over the African savanna plains
(MOCAGE and INCA excluded), regions with intense biomass burning (van der Werf et al., 2006) and
soil NO_x emissions (Yienger and Levy 1995; Vinken et al., 2014). The O_3 concentrations used to generate
365 the TransCom OH field were larger in the Southern Tropics than in the Northern latitudes (Spivakovsky
et al., 2000), in contrast to recent observations (Cooper et al., 2014). Therefore, TransCom shows the
highest [OH] over the Southern Tropics during biomass burning seasons (Spivakovsky et al., 2000) and
thus a lower N/S ratio.

370 Despite consistency on high OH values over regions influenced by human activities and biomass burning, models show the largest discrepancies over some natural ecosystem such as tropical rainforests (Fig.S2). For example, INCA, CESM, HadGEM3-Es, MRI-ESM1r1, MOCAGE and GEOSCCM simulated overall low [OH] (4×10^5 - 14×10^5 molec cm^{-3}) over tropical rainforests, despite differences in details, while EMAC, CMAM, SOCOL3 and UMUKCA-UCAM simulated overall high [OH] (16×10^5 - more than 375 25×10^5 molec cm^{-3}). Tropospheric mean [OH] over the Amazon forest show the largest variations of $>5.0 \times 10^5$ molec cm^{-3} , count for more than 50% of the multi-model mean (Fig.S2). In a more diffuse way, high latitudes of the northern hemisphere also contribute to model spread (25-35% of the model mean, Fig. S2). Besides these, inter-model differences also exist over the open ocean (up to 25% of the model mean, Fig.S2). Most simulated OH fields show higher concentrations over continents or coastal areas due to 380 higher precursor emissions, while MRI-ESM1r1, EMAC, and GEOSCCM also simulated high values ($>15 \times 10^5$ molec cm^{-3}) over the open ocean. Factors contributing to these inter-model differences are further discussed in Sect. 3.3

3.2 Vertical distributions

385 Figure 3 shows the vertical distribution of OH fields and Table 4 provides the volume-weighted mean [OH] averaged over the troposphere and over three pressure latitudinal intervals representing the planetary boundary layer, the mid-troposphere, and the upper troposphere (surface-750, 750-500, and 500-250 hPa, respectively). At the global scale, the mean tropospheric concentration of TransCom OH increases by a factor of nearly two from the surface (7×10^5 molec cm^{-3}) to 600hPa (13×10^5 molec cm^{-3}) and then 390 decreases rapidly with altitude (7×10^5 molec cm^{-3} at 250hPa). UMUKA-UCAM, HadGEM3-ES, CMAM, MOCAGE, and SOCOL3 on the other hand all show a continuous decrease of [OH] with altitude from the surface to the upper troposphere (e.g. the global mean concentrations of MOCAGE OH decreases from 23.6×10^5 molec cm^{-3} at the surface to 6.4×10^5 molec cm^{-3} at 250hPa). Other OH profiles show much

395 smaller vertical variations in the troposphere (standard deviations of mean value below 200hPa $< 2 \times 10^5$ molec cm⁻³).

Model simulated OH vertical distributions can also be different over land versus ocean (Fig. 3) and between the different latitudinal bands (Fig. S3). For example, SOCOL3 [OH] continuously decreases with altitude over both, land and ocean; MOCAGE OH increases from the surface (14.9×10^5 molec cm⁻³) to 800hPa (18.2×10^5 molec cm⁻³) and then decreases over land but almost continuously decreases over the ocean; CMAM and UMUKCA-UCAM only show significant vertical variations in [OH] over land. Vertical variations of most OH fields can be attributed to mid and low latitude regions, except for those of SOCOL3 and MOCAGE, that also decrease with altitude over mid and high northern latitudes (45°N -90°N, see Fig. S3).

405

3.3 Factors contributing to inter-model differences

Tropospheric OH is produced primarily through the reaction of O(¹D) with H₂O and secondarily through the reaction of NO with HO₂ and RO₂, and is removed primarily by reacting with CO and CH₄ (Logan et al., 1981). Hence, factors controlling inter-model OH discrepancies can be complex as differences in model emissions, chemistry, and dynamics can together impact [OH]. Here we propose a qualitative analysis focusing on both, emissions and chemical mechanisms. A more quantitative analysis would require a detailed model output of production and loss pathways and is beyond the scope of this work.

415 To analyze inter-model differences in OH vertical distributions, we compared CO, NO, and O₃ mixing ratios in table 5 as well as O(¹D) photolysis rates and specific humidity in Table S4. The inter-model variations (calculated as standard deviation/multi-model mean) in tropospheric O(¹D) photolysis rates, specific humidity, and CO mixing ratios are usually <10%-20%, while NO mixing ratios show a larger variation of 38% (12-32pptv). MRI-ESM1r1 simulated the highest NO tropospheric mixing ratio, mainly

attributable to high values above 250hPa, where OH formation is limited by H₂O. In addition, MRI-
420 ESM1r1 has ~20% more CO emissions than MOCAGE and GEOSCCM (Fig. S5), leading to about 10
ppbv higher CO mixing ratios, offsetting (for [OH]) its higher NO_x emissions and NO mixing ratios. The
high NO mixing ratios near the surface and mid-troposphere simulated by SOCOL3 (48 pptv below
750hPa and 10 pptv from 750 to 500hPa), MOCAGE (26 pptv below 750hPa and 14 pptv from 750 to
500hPa) and CMAM (17 ppbv below 750hPa) are consistent with their high tropospheric and near-surface
425 [OH]. Tropospheric O₃ can also influence primary production of OH, and tropospheric O₃ burden reflects
combined effects of NO_x, CO, and VOCs. The high O₃ over the lower troposphere simulated by SOCOL3
and low the O₃ over upper troposphere simulated by MOCAGE can contribute to explain the high and
low [OH] simulated the two models over the corresponding altitudes, respectively.

430 Lighting NO_x, which are mainly emitted in the middle and upper troposphere, can contribute to inter-
model differences in NO and OH distributions (Murray et al., 2013; 2014). We compare lightning NO_x
emissions calculated by CCM1 models in Table S3. High lightning NO_x emissions simulated by MRI-
ESM1r1 above 250hPa can explain high NO mixing ratios and increasing OH with altitude over the upper
troposphere for this model (Fig.3.). However, High NO mixing ratios in the lower troposphere simulated
435 by MOCAGE and SOCOL3 are not corresponding to high lightning NO_x emissions for these models.
Besides emissions, previous studies have reported additional factors leading to high surface NO and NO₂.
The overestimation of NO by MOCAGE could be due to the lack of N₂O₅ heterogeneous hydrolysis on
tropospheric aerosol, which is an efficient sink for NO_x (Teyss èdre et al., 2007). SOCOL3 does not include
N₂O₅ heterogeneous hydrolysis and also overestimates tropospheric NO production by NO₂ photolysis
440 compared to other models, due to issues with the look-up tables used in the calculation of photolysis rates
(Revell et al. 2018). We conclude here that physical and chemical processes related to NO production and
loss can have a large impact on OH burden and its vertical distribution. In this context, an improved
representation of the partitioning between NO and other nitrogen species in the models seems of great

importance to correctly simulate tropospheric [OH].

445

Concerning the spatial distributions, as aforementioned in Sect. 3.1, the largest model discrepancies are found over tropical rain forests. The [OH] over tropical rainforest regions are mostly sensitive to natural emissions including NO_x and NMVOCs, which vary among the models. Previous studies showed that [OH] is more sensitive to soil and lightning emissions than to wildfires, because the former sources only emit NO_x (OH source), whereas the latter emits NO_x, CO and VOCs together (OH sources and OH sinks, see Murray et al., 2014). Soil NO_x emissions in CCMI models range from around 4 Tg N yr⁻¹ in MOCAGE to more than 7 Tg N yr⁻¹ in GEOSCCM and 9Tg N yr⁻¹ in CMAM (Naik et al., 2013; Yienger and Levy, 1995); Lightning NO_x emissions range from 3.7-10.2 Tg yr⁻¹(table S3). In particular, lower NO_x emissions over South America and Africa in MOCAGE might be linked to lower [OH] over this region (Fig. S5). Isoprene and other NMVOCs remove about 3% and 7% of tropospheric OH on a global scale, respectively (Spivakovsky et al., 2000; Murray et al., 2014) and can be more important over tropical regions with higher emission rates (Sindelarova et al., 2014). The higher [OH] over tropical rainforests simulated by CMAM and UMUKCA-UCAM may be due to a lack of or the lower OH destruction by VOCs in these models. Therefore, the inter-model differences in OH spatial distributions over tropical rainforests may result from differences in natural emissions of VOC species and different related chemical reactions. The stratospheric ozone can contribute to inter-model OH discrepancies through influencing O(¹D) photolysis rates. However, we find that models that simulated lower stratosphere and total ozone column are not corresponding to higher O(¹D) photolysis rates and [OH] (table S5 and Fig. S4), since differences in photolysis schemes coupled to CCMI models can also influence the calculation of O(¹D) photolysis rates(Sukhodolov et al., 2016).

465

3.4 Inter-annual variations of OH

Figure 4 shows the time series of volume-weighted tropospheric mean [OH] from 1960 to 2010 (from

REF-C1 CCMI comparison). During this period, all OH fields show small year-to-year variations of
470 $1.9 \pm 1.2\%$, remaining within $\pm 0.5 \times 10^5$ molec cm^{-3} . CCMI models simulated significantly different OH
long-term evolutions from 1960 to 1980. For example, [OH] continuously decrease in the CMAM and
HadGEM3-ES simulations ($\sim -0.3 \times 10^5$ molec cm^{-3} ; -3.4%); and increase in SOCOL3 ($\sim +0.6 \times 10^5$ molec
 cm^{-3} ; $+4.5\%$), UMUKCA-UCAM ($\sim +0.5 \times 10^5$ molec cm^{-3} ; $+4.8\%$), and MOCAGE ($\sim +0.5 \times 10^5$ molec cm^{-3} ;
475 $+4.8\%$) during 1960-1980, while other models show no obvious long-term trend. After 1980 (1990 for
CMAM), all models show stabilized or slightly increasing [OH]. For our period of interest (after 2000)
and focusing on the anomaly in [OH] compared to the 2000-2010 mean (Fig. 4b), OH year-to-year
variations are found to be smaller than in previous decades and [OH] only increases by about $0.1\text{-}0.3 \times 10^5$
molec cm^{-3} from 2000 to 2010.

480 Previous atmospheric chemistry model studies have concluded that anthropogenic activities lead to only
a small perturbation of the OH burden, as the increased OH production tend to be compensated by an
increased loss through reactions with CO and CH₄ (Lelieveld et al., 2000; Naik et al., 2013). By
combining factors that influencing OH, Nicely et al. (2018) modeled a small inter-annual variability of
1.6% during 1980-2015. The year-to-year variations of most CCMI and INCA OH fields are consistent
485 with Nicely et al. (2018), but much smaller than the OH inter-annual variability based on MCF
observations (e.g. Bousquet et al., 2005; Montzka et al., 2011), which can reach $8.5 \pm 1.0\%$ from 1980 to
2000, and $2.3 \pm 1.5\%$ from 1998 to 2007, as compared to $2.1 \pm 0.8\%$ and $1.0 \pm 0.5\%$ here for these two
periods. As for OH trend, the ensemble of ACCMIP models simulated large divergent OH changes (even
in their signs) from 1850 to 2000, but revealed a consistent and significant increase of $3.5 \pm 2.2\%$ from
490 1980 to 2000 (Naik et al., 2013). Here, for the same period the increase of CCMI [OH] is $4.6 \pm 2.4\%$,
consistent with the ACCMIP project (Naik et al., 2013) and with other atmospheric chemistry model
studies (Dentener et al., 2003; John et al., 2012; Holmes et al., 2013; Dalsøren et al., 2016). The slightly
increasing [OH] after 2000 inferred here as well as previous model simulations (e.g. Nicely et al., 2018)

cannot help to explain stalled and renewed CH₄ growth during the 2000s, as opposed to the decreasing in
495 [OH] from mid-2000s calculated by Rigby et al. (2017) and Turner et al (2107) based on MCF
observations.

We further analyzed regional [OH] trends from 2000 to 2010 in Fig. 5. Instead of dividing subdomains as
Naik et al. (2013) did, we calculated the trend for each model grid-cell to identify and distinguish regions
500 with different trends. Most models show significant positive [OH] trends over tropical regions (0.05 -
 $0.1 \times 10^5 \text{ molec cm}^{-3} \text{ yr}^{-1}$) and over East and Southeast Asia ($>0.1 \times 10^5 \text{ molec cm}^{-3} \text{ yr}^{-1}$). By comparing
spatial distribution of OH trend with specific humidity (Fig.S6a), NO_x and CO emissions (Fig. S6b), and
stratosphere O₃ column trend, we find that positive OH trend over tropical regions are mainly
corresponding to increases in water vapor (Fig. S6a) while faster NO_x emission increases ($>5\% \text{ yr}^{-1}$) than
505 CO ($<2\% \text{ yr}^{-1}$) are consistent with positive OH trend over East and Southeast Asia (Fig. S6b). From 2000
to 2010, NO_x emissions in the MACCity (RCP85) inventory increased by 83% over East Asia, which is
much larger than the CO increase (8%) (Riahi et al., 2011). Over the rest of the extra-tropical regions such
as North America and Western Europe, the models disagree on the sign of OH change. In the Southern
hemisphere, where biogenic and fire emissions dominate, most OH fields do not show clear trends and
510 the inter-model differences are even larger. For example, MOCAGE simulated and OH decrease of >0.1
 $\times 10^5 \text{ molec cm}^{-3} \text{ yr}^{-1}$ over the Amazon, South Africa, and Indonesia, whereas MRI-ESM and EMAC-
L90MA simulated positive OH trends over these regions. CMAM and HadGEM3-ES show significant
increasing and decreasing OH trend over the Antarctic region, respectively, consistent with the significant
changes found for stratospheric O₃ (Fig. S6c).

515

In the following, we investigate how the differences in mean [OH] and variations presented in this section
affect CH₄ burden and its variations for the period 2000-2016.

4 Influences of OH fields on CH₄ simulations

520

4.1 Global total CH₄ burden

We now present the results based on the first set of LMDz experiments, where the LMDz model was run for 30 years recycling the year 2000 until the steady-state is reached. The simulations using the OH fields as given by CCMI and INCA models provide a wide range of values for the tropospheric global mean CH₄ mixing ratios (Table 6), from 1204 ppbv (SOCOL3, with a global volume-weighted tropospheric mean [OH] of 12.8×10^5 molec cm⁻³) to 1822 ppbv (INCA NMHC-AER-S, with a global volume-weighted tropospheric mean [OH] of 8.7×10^5 molec cm⁻³). It appears that the global CH₄ burden is not only sensitive to the global mean [OH], but also to its vertical distribution. Indeed, the OH radicals in the lower troposphere are more efficient to oxidize CH₄ molecules, because the CH₄+OH reaction rate increases with temperature (Eq. 1). When considering the standard atmosphere, the reaction rate corresponding to the surface temperature of 288K (5.2×10^{-15} s⁻¹) is more than twice that for the 500hPa temperature of 253K (2.2×10^{-15} s⁻¹). Despite similar volume-weighted tropospheric mean [OH] of $\sim 10.4 \times 10^5$ molec cm⁻³, MOCAGE simulated much lower CH₄ mixing ratios (1275 ppbv) than CMAM (1540 ppbv) and MRI-ESM1r1 (1639 ppbv) because of its higher near surface [OH] (19×10^5 molec m⁻³) (Table 4). Previous studies have demonstrated that the sensitivity of CH₄ oxidation to lower tropical temperature (Spivakovsky et al., 2000; John et al., 2012), and our simulations show that 36%-46% of CH₄ is oxidized over lower tropical region (surface-750hPa, 30 °S-30 °N) (Table S6). The spatial distribution of the OH radicals also slightly influences CH₄ oxidation. Indeed, the [OH] of EMAC-L90MA are higher than those of CESM-WACCM for both, tropospheric (11.1×10^5 versus 10.7×10^5 molec cm⁻³) and near-surface (12.5×10^5 versus 12.4×10^5 molec cm⁻³) means, but a slightly higher CH₄ burden is found for the former (1579 versus 1575 ppbv, Table 6). This is because EMAC-L90MA simulated higher [OH] over the ocean, while CESM-WACCM OH is more concentrated over land closer to CH₄ source regions. The model experiments also emphasize that volume-weighted tropospheric concentrations cannot fully indicate the

540

atmospheric oxidizing efficiency for CH₄, as has been discussed by Lawrence et al. (2001). Tropospheric
545 mean [OH] weighted by reaction rates with CH₄, which consider both temperature and CH₄ distributions,
can be a better indicator for CH₄ oxidation (Lawrence et al., 2001).

4.2 Impacts on CH₄ spatial distribution and growth rate

In order to address the question of inter-annual variability of atmospheric CH₄, we scaled each OH field
550 globally to get the same CH₄ loss (for the year 2000) as the one obtained with INCA NMHC OH field
(see Sect. 2.2.2). The single global scaling factor (per OH field) for the year 2000 is applied to every year
between 2000 and 2010. As listed in Table 4, after scaling most OH fields have volume-weighted
tropospheric mean concentrations closer to INCA NMHC (9.7×10^5 molec cm⁻³), within the range of 9.0-
10.4 × 10⁵ molec cm⁻³. One exception is MOCAGE, with tropospheric mean [OH] scaled to 7.7×10^5 molec
555 cm⁻³, due to its distinct vertical distribution (Sect.3.2). This scaling of OH makes it possible to start model
experiments at the same initial CH₄ burden. Although slightly modifying the magnitude of the global
mean [OH], this scaling maintained the spatial and temporal differences and trend over the 2000-2010
period.

560 4.2.1 Spatial distributions of tropospheric CH₄ mixing ratios

We used the scaled OH fields to perform simulations between 2000 and 2010. Figure 6 shows the spatial
distribution of tropospheric CH₄ mixing ratios for the simulation Run_standard (Table. 2, driven by OH
with inter-annual variations) averaged over 2000-2010. Although all simulations started from the same
initial conditions and OH fields were scaled to give the same global CH₄ loss as INCA NMHC in 2000,
565 LMDz simulations using the different scaled OH fields still generated a spread of tropospheric mean
(8ppbv) and spatial distribution of CH₄ mixing ratios averaged during 2000-2010. Differences between
the global tropospheric mean [OH] cannot explain these differences (see Table 4). Clearly the different
spatial (horizontal and vertical) and temporal variations of the OH fields (as described in Sect. 3), which

were kept in this experiment by only scaling [OH] globally, significantly modify the simulated CH₄ mixing ratios (Table 7 and Fig. 6). OH fields with increasing trend will lead to lower LMDz simulated CH₄ mixing ratios. The LMDz simulations using the TransCom OH fields (without inter-annual variability) shows the highest CH₄ mixing ratios (1735 ppbv), while the one using the CMAM OH (with slightly increasing OH trend during the decade) shows the lowest mixing ratios (1727 ppbv).

The differences in spatial distribution of OH fields can influence LMDz simulated CH₄ spatial distributions. Looking at latitudinal CH₄ mixing ratios, the inter-model differences appear larger than in the global mean (Fig. 6 and Table 7). The model spreads of the mean CH₄ mixing ratios over 60°S-90°S and 60°N-90°N range from 1771 to 1794ppbv and 1784 to 1812ppbv, respectively. Here, we define the N/S gradient of CH₄ as the difference in mean CH₄ mixing ratio between the latitudinal bands 60°N - 90°N and from 60°S - 90°S. With the TransCom OH field (N/S ratio =1.0), the model simulated 12-43% larger N/S gradients of CH₄ (129 ppbv) than other simulations (90-115 ppbv) driven by OH fields with higher N/S OH ratios of 1.2-1.5. Previous model studies have attributed the overestimation of the CH₄ N/S ratio to an underestimation of model inter-hemispheric exchange time (e.g. Zimmermann et al., 2018). Our results show that uncertainties in OH distributions can also contribute to such model biases.

4.2.2 Changes in CH₄ mixing ratios

To assess the influence of OH inter-annual variations on CH₄ mixing ratios, we calculated the difference in the simulated CH₄ between the standard run (Run_standard) and the simulations with fixed [OH] (Run_fix_OH, Table 2). The Run_fix_OH simulations show that global tropospheric mean CH₄ mixing ratios increased by 75 ppbv from 2000 to 2010 (Fig. 7, black dashed lines), due to the enhanced emissions (Fig.1). The increase in [OH] can obviously reduce CH₄ growth. An increase in [OH] by 0.1-0.3 × 10⁵ molec cm⁻³ (1%-3%) (Fig. 7, orange lines) during this period leads to a reduction of the CH₄ mixing ratios by 5-15 ppbv by 2010 (Fig. 7, blue lines). The largest reductions are found when using CESM1-WACCM

and CMAM OH fields, given the continuous OH growth in these models. Compared to Run_fix_OH, we
595 estimated that such reductions in CH₄ mixing ratios offset 7- 20% of the CH₄ increase driven by the rising
CH₄ emissions of our scenario over the period 2000 to 2010.

To test whether the impacts of [OH] year-to-year variations on CH₄ mixing ratios the chosen emission
scenarios, we compare the above results with that calculated by an extreme scenario where model
600 simulations are driven by fixed emission(year 2000, Run_fix_emis and Run_fix_emis_OH, table 2). With
emissions fixed to 2000, the CH₄ mixing ratio increased by 2ppbv from 2000 to 2010, and increasing OH
(CESM-WACCM OH fields) can reduce CH₄ mixing ratio by 13.5ppb in 2010, comparable to 13.9 ppb
calculated by Run_std and Run_fix_OH with CESM-WACCM OH fields. The results indicate only a
small effect of emission scenario choices on the absolute changes of CH₄ mixing ratios due to OH
605 variations. However, our choices have a large effect on relative change to the total modeled CH₄ increase.
Indeed, if we use the emission scenarios that match observations (~+25ppbv of CH₄ mixing ratio increase
from 2000-2010, Ed Dlugokencky, NOAA/ESRL, 2019) instead of ~70ppb here , the CH₄ mixing ratio
changes due to OH can contribute to more than half (13.5-13.9ppbv versus 25ppbv) of the changes driven
by emissions.

610 After 2010, CCM1 REF-C2 experiments simulated increasing, relatively stable, or decreasing OH
variations, thus having a variable influence on CH₄ variations. Over the period 2011-2016, [OH]
simulated by EMAC-L90MA, CESM-WACCM and CMAM stabilizes at a level $0.2-0.4 \times 10^5$ molec cm⁻³
higher than the concentrations in 2000, further reducing CH₄ mixing ratios by up to 20-30 ppbv in 2016
615 (Fig. 7, blue lines). Other OH fields have similar concentrations over 2010-2016 as in the early 2000s
(Fig. 7, orange lines), thus simulating CH₄ mixing ratios that remain close to Run_fix_OH with
differences less than a few +/-ppbv.

As large uncertainties remain regarding the inter-annual variations and trend of OH after 2010, we have
620 tested two additional OH scenarios: Run_OH_inc (with an annual increase of $0.1\% \text{ yr}^{-1}$) and Run_OH_dec
(with an annual decrease of $1\% \text{ yr}^{-1}$), to assess the uncertainty range of the impact of OH changes (the
orange areas in Fig. 7) on CH₄ mixing ratios (the blue areas in Fig. 7). In these two scenarios, the mean
[OH] of run_OH_dec is $\sim 7 \times 10^5 \text{ molec cm}^{-3}$ (7%) lower than run_OH_inc in 2016 relative to the
Run_fix_OH. If OH decreases at $1\% \text{ yr}^{-1}$ after 2010, by 2016, the differences in CH₄ mixing ratios
625 between Run_OH_dec and Run_fix_OH range -7 – 30 ppbv, with the lower end (-7 ppbv) simulated by OH
from CESM1-WACCM given its highest [OH] in 2010. On the contrary, Run_OH_inc simulated 3 – 39
ppbv lower CH₄ mixing ratios compared to Run_fix_OH (the blue areas in Fig. 7). As such, uncertainties
in the OH trend can clearly lead to $> \pm 30$ ppbv changes in CH₄ mixing ratios (the gray areas in Fig. 7)
after only 6 years of simulations, as compared to the fix-OH case.

630

It is now interesting to compare the range of simulated [CH₄] changes induced by OH scenarios to changes
in surface CH₄ observations, in order to quantify how much of the model-observation mismatch could
potentially be attributed to uncertainties in [OH] and its variability (Fig. 8). To do so, we used surface
CH₄ observations from the National Oceanic and Atmospheric Administration (NOAA) networks and
635 selected stations with 17 years continuous records over 2000-2016. The modeled surface CH₄ mixing
ratios are sampled according to station locations. Since the simulated absolute CH₄ mixing ratios largely
depend on the initial conditions and OH fields, we compared changes in the simulated and observed global
CH₄ mixing ratios starting at the same point in 2000. The observed CH₄ shows zero growth between 2000
and 2006 and then increases by 5.6 ppbv yr^{-1} between 2006 and 2012 (6.4 ppbv yr^{-1} for 2006-2010) and by
640 9.4 ppbv yr^{-1} after 2012 (Fig. 8). In this study we do not expect to fit these CH₄ trends as this inter-
comparison was not conducted with a set of optimized emissions. It has already been noticed that standard
CH₄ emission inventories lead to overestimated CH₄ mixing ratios (e.g. Saunio et al., 2016). Indeed,
neither Run_standard nor Run_fix_OH simulations do capture the stagnation during 2003-2006, and

overestimated surface CH₄ increments by 2.5-5.2 ppbv yr⁻¹ during the period 2006-2010. We define
645 highest CH₄ mixing ratios simulated by different OH as CH_{4-H}, lowest CH₄ mixing ratios as CH_{4-L}, and
CH₄ simulated by Run_fix_OH as CH_{4-fix_OH}. Based on Run_fix_OH, on average over 2000-2016 and
depending on the OH scenario, we found that [OH] changes can emphasize the model-observation
mismatch by up to 19% (mean values of $(\text{CH}_{4\text{-H}} - \text{CH}_{4\text{-fix_OH}}) / (\text{CH}_{4\text{-fix_OH}} - \text{observed CH}_4)$) during 2000-
2016), or limit the model-observation mismatch by up to 54% (mean values of $(\text{CH}_{4\text{-fix_OH}} - \text{CH}_{4\text{-}}$
650 $\text{fix_L}) / (\text{CH}_{4\text{-fix_OH}} - \text{observed CH}_4)$) during 2000-2016) (figure 8). Such comparisons strongly suggest that
a better understanding of OH inter-annual variations and trends is required in order to simulate more
reliable CH₄ trends in atmospheric chemistry models. Atmospheric chemistry transport model (Dalsøren
et al., 2016) and box model studies (Rigby et al., 2017; Turner et al., 2017) have pointed out that variations
in OH can partly explain the recent CH₄ trends. However, current top-down estimates of CH₄ emissions
655 usually assume constant [OH] (Saunois et al., 2017) and attribute the model-observation discrepancies
only to surface emissions rather than changes in [OH]. Our results confirm the potentially significant role
played by the still uncertain OH changes in the actual changes of methane emissions since 2000.

5 Conclusions

660

We have analyzed 14 OH fields (11 from CCMI experiments, 2 from INCA model simulations, 1 from
TransCom) to investigate the inter-model differences in the spatial distributions and trends of tropospheric
OH, and estimated the influences of OH spatio-temporal distributions on tropospheric CH₄ by feeding
them in different simulations with LMDz offline chemistry transport model.

665

Simulated global volume-weighted tropospheric mean [OH] are within the range of 8.7×10^5 - 12.8×10^5
molec cm⁻³, which is consistent with the (large) multi-model range of previous estimates. CCMI and
INCA models simulated larger [OH] in the Northern hemisphere than in the Southern hemisphere (N/S

ratio of 1.2-1.5), with consistently high OH values over anthropogenic emission hotspots in North
670 America, East and South East Asia, while TransCom OH shows a N/S ratio close to 1.0. In the vertical,
TransCom OH reaches its maximum value at about 600 hPa, while CCMI and INCA OH fields either
continuously decrease with altitude or show very small vertical variations in the troposphere. The factors
most likely responsible for these inter-model differences include i) large NO mixing ratios leading to high
surface and mid-tropospheric [OH] (Teyss re et al., 2007; Pevell et al. 2018), and ii) different natural
675 emissions as well as VOC species and chemical mechanisms driving spatial model discrepancies over
natural ecosystems.

Simulated OH fields show small year-to-year variations, within $\pm 0.5 \times 10^5$ molec cm^{-3} during 1960-2010.
From 2000 to 2010, year-to-year variations in OH are smaller than in previous decades and all OH fields
680 increase by about $0.01-0.03 \times 10^5$ molec $\text{cm}^{-3} \text{yr}^{-1}$. Such an increase in OH is mainly attributed to the
significant positive OH trend over East and Southeast Asia ($>0.1 \times 10^5$ molec $\text{cm}^{-3} \text{yr}^{-1}$) in response to more
OH production by NO_x than OH destruction by CO, and over tropical regions in response to increasing
water vapor.

685 The inter-model differences in tropospheric OH burden generate a wide range of CH_4 burdens (1204-
1882ppbv) when used to simulate steady-state CH_4 mixing ratios in the atmospheric chemistry model
LMDz. Our findings suggest that not only different global mean [OH], but also differences in the
horizontal and vertical distributions between OH fields are responsible for this range (CH_4 destruction
rates by OH increase with temperature).

690 The CH_4 simulations for 2000-2016 using OH with inter-annual variation show that inter-model
differences of the OH N/S ratio lead to 12-43% differences in the CH_4 N/S gradient. For the time period
2000-2010, we found that a 1%-3% increase in [OH] leads to a 5-15 ppb reduction of the CH_4 mixing

ratio until 2010, accounting for 7-20% of the simulated emission driven CH₄ increase over this period.
695 After 2010, the ensemble of OH scenarios tested here leads to differences in CH₄ mixing ratio of up to 30
ppb by 2016. Comparing with surface observations, we found that [OH] changes can emphasize the
model-observation mismatch by up to 19%, or fill the gap between model simulations and observations
by up to 54% (Figure 8). Therefore, addressing the OH variability in CH₄ source inversions seems critical
to avoid a wrong attribution of CH₄ changes to emission changes only. Future work is needed to quantify
700 the impact of this ensemble of OH fields on CH₄ emissions obtained by inversion and to generate
improved OH fields to be used in CH₄ inversion studies.

Author contributions

YZ, MS, and PB designed the study, analyzed data and wrote the manuscript. BZ and XL helped with
705 data analysis and model simulations. JC, RJ, and AS discussed the results. ED provided the atmospheric
in situ data. Other co-authors provided numerical model outputs. All co-authors commented on the
manuscript.

Acknowledgements

710 This work has been funded by the Gordon and Betty Moore Foundation through Grant GBMF5439
'Advancing Understanding of the Global Methane Cycle' and takes benefit of the expertise of the Global
Carbon Project methane initiative.

We acknowledge the modelling groups for making their simulations available for this analysis, the joint
WCRP SPARC/IGAC Chemistry-Climate Model Initiative (CCMI) for organising and coordinating the
715 model data analysis activity, and the British Atmospheric Data Centre (BADC) for collecting
and archiving the CCMI model output.

The EMAC simulations have been performed at the German Climate Computing Centre (DKRZ) through
support from the Bundesministerium für Bildung und Forschung (BMBF). DKRZ and its scientific

steering committee are gratefully acknowledged for providing the HPC and data archiving resources for
720 this consortial project ESCiMo (Earth System Chemistry integrated Modelling).

The CESM project is supported primarily by the National Science Foundation.

Eugene Rozanov work is partially supported by Swiss national Science Foundation under grant
200020_182239 (POLE) and the gained information will be used to improve next versions of the CCM
SOCOL.

725 Andrea Stenke was supported by the Swiss National Science Foundation under grant 200021_138037
(FuMES).

UMUKCA-UCAM model integrations were performed using the ARCHER UK National
Supercomputing Service and MONSooN system, a collaborative facility supplied under the Joint Weather
and Climate Research Programme, which is a strategic partnership between the UK Met Office and the
730 Natural Environment Research Council.

References

Allen, D. J., and Pickering, K. E.: Evaluation of lightning flash rate parameterizations for use in a global
chemical transport model, *Journal of Geophysical Research: Atmospheres*, 107, ACH 15-11-ACH 15-21,
735 doi:10.1029/2002JD002066, 2002.

Bednarz, E. M., Maycock, A. C., Abraham, N. L., Braesicke, P., Dessens, O., and Pyle, J. A.: Future
Arctic ozone recovery: the importance of chemistry and dynamics, *Atmos. Chem. Phys.*, 16, 12159–
12176, doi:10.5194/acp-16-12159-2016, 2016.

Bousquet, P., Hauglustaine, D. A., Peylin, P., Carouge, C., and Ciais, P.: Two decades of OH variability
as inferred by an inversion of atmospheric transport and chemistry of methyl chloroform, *Atmos. Chem.*
740 *Phys.*, 5, 2635-2656, doi:10.5194/acp-5-2635-2005, 2005.

Archibald, A. T., Levine, J. G., Abraham, N. L., Cooke, M. C., Edwards, P. M., Heard, D. E., Jenkin, M.
E., Karunaharan, A., Pike, R. C., Monks, P. S., Shallcross, D. E., Telford, P. J., Whalley, L. K., and Pyle,
J. A.: Impacts of HO_x regeneration and recycling in the oxidation of isoprene: Consequences for the
745 composition of past, present and future atmospheres, *Geophysical Research Letters*, 38, L05804,
doi:10.1029/2010GL046520, 2011. Bousquet, P., Ringeval, B., Pison, I., Dlugokencky, E. J., Brunke, E.
G., Carouge, C., Chevallier, F., Fortems-Cheiney, A., Frankenberg, C., Hauglustaine, D. A., Krummel, P.
B., Langenfelds, R. L., Ramonet, M., Schmidt, M., Steele, L. P., Szopa, S., Yver, C., Viovy, N., and Ciais,

- P.: Source attribution of the changes in atmospheric methane for 2006–2008, *Atmospheric Chemistry and Physics*, 11, 3689-3700, doi:10.5194/acp-11-3689-2011, 2011.
- 750 Brenninkmeijer, C. A. M., Manning, M. R., Lowe, D. C., Wallace, G., Sparks, R. J., and Volz-Thomas, A.: Interhemispheric asymmetry in OH abundance inferred from measurements of atmospheric ^{14}CO , *Nature*, 356, doi:50, 10.1038/356050a0, 1992.
- Ciais, P., Sabine, C., Bala, G., Bopp, L., Brovkin, V., al, e., and House, J. I.: Carbon and Other Biogeochemical Cycles, in: *Climate Change 2013: The Physical Science Basis. Contribution of Working Group I to the Fifth Assessment Report of the Intergovernmental Panel on Climate Change*, Cambridge University Press, Cambridge, United Kingdom and New York, NY, USA., 2013.
- 755 Colin, P., and David, R.: Possible implications of global climate change on global lightning distributions and frequencies, *Journal of Geophysical Research: Atmospheres*, 99, 10823-10831, doi:10.1029/94JD00019, 1994.
- 760 Dee, D. P., Uppala, S. M., Simmons, A. J., Berrisford, P., Poli, P., Kobayashi, S., Andrae, U., Balmaseda, M. A., Balsamo, G., Bauer, P., Bechtold, P., Beljaars, A. C. M., van de Berg, L., Bidlot, J., Bormann, N., Delsol, C., Dragani, R., Fuentes, M., Geer, A. J., Haimberger, L., Healy, S. B., Hersbach, H., Hód, E. V., Isaksen, I., Kållberg, P., Köhler, M., Matricardi, M., McNally, A. P., Monge-Sanz, B. M., Morcrette, J.-J., Park, B.-K., Peubey, C., de Rosnay, P., Tavolato, C., Thépaut, J.-N., and Vitart, F.: The ERA-Interim reanalysis: configuration and performance of the data assimilation system, *Quarterly Journal of the Royal Meteorological Society*, 137, 553-597, doi:10.1002/qj.828, 2011.
- 765 Ed Dlugokencky, NOAA/ESRL, www.esrl.noaa.gov/gmd/ccgg/trends_ch4/, 2018
- Emanuel, K. A.: A Scheme for Representing Cumulus Convection in Large-Scale Models, *Journal of the Atmospheric Sciences*, 48, 2313-2329, doi:10.1175/1520-0469(1991)048<2313:ASFRCC>2.0.CO;2, 1991.
- 770 Cooper, O. R., Parrish, D. D., Ziemke, J., Balashov, N. V., Cupeiro, M., Galbally, I. E., Gilge, S., Horowitz, L., Jensen, N. R., Lamarque, J. F., Naik, V., Oltmans, S. J., Schwab, J., Shindell, D. T., Thompson, A. M., Thouret, V., Wang, Y., and Zbinden, R. M.: Global distribution and trends of tropospheric ozone: An observation-based review, *Elementa: Science of the Anthropocene*, 2, 000029, doi: 10.12952/journal.elementa.000029, 2014.
- 775 Crutzen, P.: A discussion of the chemistry of some minor constituents in the stratosphere and troposphere, *Pure and Applied Geophysics*, 106, 1385-1399, doi: 10.1007/bf00881092, 1973.
- Dalsøren, S. B., Myhre, C. L., Myhre, G., Gomez-Pelaez, A. J., Søvde, O. A., Isaksen, I. S. A., Weiss, R. F., and Harth, C. M.: Atmospheric methane evolution the last 40 years, *Atmospheric Chemistry and Physics*, 16, 3099-3126, doi:10.5194/acp-16-3099-2016, 2016.
- 780 Dentener, F., Peters, W., Krol, M., van Weele, M., Bergamaschi, P., and Lelieveld, J.: Interannual variability and trend of CH_4 lifetime as a measure for OH changes in the 1979–1993 time period, *Journal of Geophysical Research: Atmospheres*, 108, 4442, 10.1029/2002jd002916, 2003.
- 785 Deushi, M. and Shibata, K.: Development of a Meteorological Research Institute chemistry-climate

- model version 2 for the study of tropospheric and stratospheric chemistry, *Pap. Meteorol. Geophys.*, 62, 1–46, 2011.
- EHHALT, D. H.: The atmospheric cycle of methane, *Tellus*, 26, 58-70, doi:10.1111/j.2153-3490.1974.tb01952.x, 1974.
- 790 Etminan, M., Myhre, G., Highwood, E. J., and Shine, K. P.: Radiative forcing of carbon dioxide, methane, and nitrous oxide: A significant revision of the methane radiative forcing, *Geophysical Research Letters*, 43, 12,614-612,623, doi:10.1002/2016GL071930, 2016.
- Etiopé, G.: Natural Gas Seepage: The Earth's Hydrocarbon Degassing, in, Springer International Publishing, Cham, 195 pp., 2015.
- 795 Garcia, R. R. and Boville, B. A.: Downward control of the meanmeridional circulation and temperature distribution of the polar winter stratosphere, *J. Atmos. Sci.*, 51, 2238–2245, 1994.
- Granier, C., Bessagnet, B., Bond, T., D'Angiola, A., Denier van der Gon, H., Frost, G. J., Heil, A., Kaiser, J. W., Kinne, S., Klimont, Z., Kloster, S., Lamarque, J.-F., Liousse, C., Masui, T., Meleux, F., Mieville, A., Ohara, T., Raut, J.-C., Riahi, K., Schultz, M. G., Smith, S. J., Thompson, A., van Aardenne, J., van
800 der Werf, G. R., and van Vuuren, D. P.: Evolution of anthropogenic and biomass burning emissions of air pollutants at global and regional scales during the 1980–2010 period, *Climatic Change*, 109, 163, doi:10.1007/s10584-011-0154-1, 2011.
- Grewe, V., Brunner, D., Dameris, M., Grenfell, J. L., Hein, R., Shindell, D., and Staehelin, J.: Origin and variability of upper tropospheric nitrogen oxides and ozone at northern mid-latitudes, *Atmospheric
805 Environment*, 35, 3421-3433, [https://doi.org/10.1016/S1352-2310\(01\)00134-0](https://doi.org/10.1016/S1352-2310(01)00134-0), 2001.
- Guth, J., Josse, B., Maréchal, V., Joly, M., and Hamer, P.: First implementation of secondary inorganic aerosols in the MOCAGE version R2.15.0 chemistry transport model, *Geosci. Model Dev.*, 9, 137–160, doi:10.5194/gmd-9-137-2016, 2016.
- Hardiman, S. C., Butchart, N., O'Connor, F. M., and Rumbold, S. T.: The Met Office HadGEM3-ES
810 chemistry–climate model: evaluation of stratospheric dynamics and its impact on ozone, *Geosci. Model Dev.*, 10, 1209-1232, doi: 10.5194/gmd-10-1209-2017, 2017.
- Hauglustaine, D. A., Hourdin, F., Jourdain, L., Filiberti, M.-A., Walters, S., Lamarque, J.-F., and Holland, E. A.: Interactive chemistry in the Laboratoire de Mééorologie Dynamique general circulation model: Description and background tropospheric chemistry evaluation, *Journal of Geophysical Research:
815 Atmospheres*, 109, doi:10.1029/2003JD003957, 2004.
- Holmes, C. D., Prather, M. J., Søvde, O. A., and Myhre, G.: Future methane, hydroxyl, and their uncertainties: key climate and emission parameters for future predictions, *Atmospheric Chemistry and Physics*, 13, 285-302, 10.5194/acp-13-285-2013, 2013.
- Hourdin, F., and Armengaud, A.: The Use of Finite-Volume Methods for Atmospheric Advection of Trace
820 Species. Part I: Test of Various Formulations in a General Circulation Model, *Monthly Weather Review*, 127, 822-837, doi:10.1175/1520-0493(1999)127<0822:tuofvm>2.0.co;2, 1999.
- Hourdin, F., Mauritsen, T., Gettelman, A., Golaz, J.-C., Balaji, V., Duan, Q., Folini, D., Ji, D., Klocke, D.,

- 825 Qian, Y., Rauser, F., Rio, C., Tomassini, L., Watanabe, M., and Williamson, D.: The Art and Science of Climate Model Tuning, *Bulletin of the American Meteorological Society*, 98, doi:589-602, 10.1175/bams-d-15-00135.1, 2017.
- Janssens-Maenhout, G., Crippa, M., Guizzardi, D., Muntean, M., Schaaf, E., Dentener, F., Bergamaschi, P., Pagliari, V., Olivier, J. G. J., Peters, J. A. H. W., van Aardenne, J. A., Monni, S., Doering, U., and Petrescu, A. M. R.: EDGAR v4.3.2 Global Atlas of the three major Greenhouse Gas Emissions for the period 1970-2012, *Earth Syst. Sci. Data Discuss.*, 2017, 1-55, doi:10.5194/essd-2017-79, 2017.
- 830 Jourdain, L., Bekki, S., Lott, F., and Lefèvre, F.: The coupled chemistry-climate model LMDz-REPROBUS: description and evaluation of a transient simulation of the period 1980–1999, *Ann. Geophys.*, 26, 1391-1413, doi: 10.5194/angeo-26-1391-2008, 2008.
- Hegglin, M. I. and Lamarque, J.-F.: The IGAC/SPARC Chemistry-Climate Model Initiative Phase-1 (CCMI-1) model data output, NCAS British Atmospheric Data Centre, [ADD ACCESS DATE], available at:<http://catalogue.ceda.ac.uk/uuid/9cc6b94df0f4469d8066d69b5df879d5>, 2015.
- 835 Hunke, E. C. and Lipscombe, W. H.: CICE: the Los Alamos sea ice model documentation and software user's manual, Version 4.0, LA-CC-06-012, Los Alamos National Laboratory, New Mexico, 2008.
- John, J. G., Fiore, A. M., Naik, V., Horowitz, L. W., and Dunne, J. P.: Climate versus emission drivers of methane lifetime against loss by tropospheric OH from 1860–2100, *Atmospheric Chemistry and Physics*, 12, 12021-12036, doi:10.5194/acp-12-12021-2012, 2012.
- 840 Jöckel, P., Kerkweg, A., Pozzer, A., Sander, R., Tost, H., Riede, H., Baumgaertner, A., Gromov, S., and Kern, B.: Development cycle 2 of the Modular Earth Submodel System (MESSy2), *Geosci. Model Dev.*, 3, 717–752, doi:10.5194/gmd-3-717-2010, 2010.
- Josse, B., Simon, P., and Peuch, V.-H.: Radon global simulations with the multiscale chemistry and transport model MOCAGE, *Tellus B*, 56, 339–356, 2004.
- 845 Jöckel, P., Tost, H., Pozzer, A., Kunze, M., Kirner, O., Brenninkmeijer, C. A. M., Brinkop, S., Cai, D. S., Dyroff, C., Eckstein, J., Frank, F., Garny, H., Gottschaldt, K.-D., Graf, P., Grewe, V., Kerkweg, A., Kern, B., Matthes, S., Mertens, M., Meul, S., Neumaier, M., Nützel, M., Oberländer-Hayn, S., Ruhnke, R., Runde, T., Sander, R., Scharffe, D., and Zahn, A.: Earth System Chemistry integrated Modelling (ESCiMo) with the Modular Earth Submodel System (MESSy) version 2.51, *Geosci. Model Dev.*, 9, 1153–1200, doi:10.5194/gmd-9-1153-2016, 2016.
- 850 Jonsson, A. I., de Grandpré J., Fomichev, V. I., McConnell, J. C., and Beagley, S. R.: Doubled CO₂-induced cooling in the middle atmosphere: Photochemical analysis of the ozone radiative feedback, *J. Geophys. Res.*, 109, D24103, doi:10.1029/2004JD005093, 2004.
- Krol, M., and Lelieveld, J.: Can the variability in tropospheric OH be deduced from measurements of 1,1,1-trichloroethane (methyl chloroform)?, *Journal of Geophysical Research: Atmospheres*, 108, doi:10.1029/2002JD002423, 2003.
- Lamarque, J. F., Bond, T. C., Eyring, V., Granier, C., Heil, A., Klimont, Z., Lee, D., Liousse, C., Mieville, A., Owen, B., Schultz, M. G., Shindell, D., Smith, S. J., Stehfest, E., Van Aardenne, J., Cooper, O. R.,

- 860 Kainuma, M., Mahowald, N., McConnell, J. R., Naik, V., Riahi, K., and van Vuuren, D. P.: Historical (1850–2000) gridded anthropogenic and biomass burning emissions of reactive gases and aerosols: methodology and application, *Atmos. Chem. Phys.*, 10, 7017-7039, doi:10.5194/acp-10-7017-2010, 2010.
- Lambert, G., and Schmidt, S.: Reevaluation of the oceanic flux of methane: Uncertainties and long term variations, *Chemosphere*, 26, 579-589, doi:https://doi.org/10.1016/0045-6535(93)90443-9, 1993.
- 865 Lawrence, M. G., Jöckel, P., and von Kuhlmann, R.: What does the global mean OH concentration tell us?, *Atmos. Chem. Phys.*, 1, 37-49, 10.5194/acp-1-37-2001, 2001.
- Lelieveld, J., and Dentener, F. J.: What controls tropospheric ozone?, *Journal of Geophysical Research: Atmospheres*, 105, 3531-3551, doi:10.1029/1999JD901011, 2000.
- Lelieveld, J., Dentener, F. J., Peters, W., and Krol, M. C.: On the role of hydroxyl radicals in the self-cleansing capacity of the troposphere, *Atmos. Chem. Phys.*, 4, 2337-2344, doi:10.5194/acp-4-2337-2004, 2004.
- 870 Lelieveld, J., Butler, T. M., Crowley, J. N., Dillon, T. J., Fischer, H., Ganzeveld, L., Harder, H., Lawrence, M. G., Martinez, M., Taraborrelli, D., and Williams, J.: Atmospheric oxidation capacity sustained by a tropical forest, *Nature*, 452, 737-740, doi:10.1038/nature06870, 2008.
- 875 Lelieveld, J., Gromov, S., Pozzer, A., and Taraborrelli, D.: Global tropospheric hydroxyl distribution, budget and reactivity, *Atmospheric Chemistry and Physics*, 16, 12477-12493, doi: 10.5194/acp-16-12477-2016, 2016.
- Levy, H.: Normal Atmosphere: Large Radical and Formaldehyde Concentrations Predicted, *Science*, 173, 141-143, 10.1126/science.173.3992.141, 1971.
- 880 Lin, X., Ciais, P., Bousquet, P., Ramonet, M., Yin, Y., Balkanski, Y., Cozic, A., Delmotte, M., Evangeliou, N., Indira, N. K., Locatelli, R., Peng, S., Piao, S., Saunois, M., Swathi, P. S., Wang, R., Yver-Kwok, C., Tiwari, Y. K., and Zhou, L.: Simulating CH₄ and CO₂ over South and East Asia using the zoomed chemistry transport model LMDz-INCA, *Atmospheric Chemistry and Physics*, 18, 9475-9497, doi:10.5194/acp-18-9475-2018, 2018.
- 885 Locatelli, R., Bousquet, P., Hourdin, F., Saunois, M., Cozic, A., Couvreux, F., Grandpeix, J. Y., Lefebvre, M. P., Rio, C., Bergamaschi, P., Chambers, S. D., Karstens, U., Kazan, V., van der Laan, S., Meijer, H. A. J., Moncrieff, J., Ramonet, M., Scheeren, H. A., Schlosser, C., Schmidt, M., Vermeulen, A., and Williams, A. G.: Atmospheric transport and chemistry of trace gases in LMDz5B: evaluation and implications for inverse modelling, *Geosci. Model Dev.*, 8, 129-150, 10.5194/gmd-8-129-2015, 2015.
- 890 Logan, J. A., Prather, M. J., Wofsy, S. C., and McElroy, M. B.: Tropospheric chemistry: A global perspective, *Journal of Geophysical Research*, 86, 7210, doi:10.1029/JC086iC08p07210, 1981.
- Lu, X., Hong, J., Zhang, L., Cooper, O. R., Schultz, M. G., Xu, X., Wang, T., Gao, M., Zhao, Y., and Zhang, Y.: Severe Surface Ozone Pollution in China: A Global Perspective, *Environmental Science & Technology Letters*, 5, 487-494, doi:10.1021/acs.estlett.8b00366, 2018.
- 895 Madec, G.: NEMO ocean engine, Institut Pierre-Simon Laplace (IPSL), France, No. 27, ISSN No. 1288-1619, 2008.

- Marsh, D., Mills, M. J., Kinnison, D. E., Garcia, R. R., Lamarque, J.-F., and Calvo, N.: Climate change from 1850–2005 simulated in CESM1 (WACCM), *J. Climate*, 26, 7372–7391, doi:10.1175/JCLI-D-12-00558.1, 2013.
- 900 Masui, T., Matsumoto, K., Hijioka, Y., Kinoshita, T., Nozawa, T., Ishiwatari, S., Kato, E., Shukla, P., Yamagata, Y., and Kainuma, M.: An emission pathway for stabilization at 6 Wm⁻² radiative forcing, *Climatic change*, 109, 59, 2011.
- McNorton, J., Chipperfield, M. P., Gloor, M., Wilson, C., Feng, W., Hayman, G. D., Rigby, M., Krummel, P. B., amp, apos, Doherty, S., Prinn, R. G., Weiss, R. F., Young, D., Dlugokencky, E., and Montzka, S. A.:
- 905 Role of OH variability in the stalling of the global atmospheric CH₄ growth rate from 1999 to 2006, *Atmospheric Chemistry and Physics*, 16, 7943-7956, 10.5194/acp-16-7943-2016, 2016.
- Miyazaki, K., Eskes, H. J., and Sudo, K.: Global NO_x emission estimates derived from an assimilation of OMI tropospheric NO₂ columns, *Atmos. Chem. Phys.*, 12, 2263-2288, doi:10.5194/acp-12-2263-2012,
- 910 2012.
- Montzka, S. A., Krol, M., Dlugokencky, E., Hall, B., Jöckel, P., and Lelieveld, J.: Small Interannual Variability of Global Atmospheric Hydroxyl, *Science*, 331, 67-69, doi:10.1126/science.1197640, 2011.
- Molod, A., Takacs, L., Suarez, M., Bacmeister, J., Song, I.-S., and Eichmann, A.: The GEOS-5 Atmospheric General Circulation Model: Mean Climate and Development from MERRA to Fortuna,
- 915 NASA Technical Report Series on Global Modeling and Data Assimilation, NASA TM-2012-104606, 28, 117 pp., 2012.
- Molod, A., Takacs, L., Suarez, M., and Bacmeister, J.: Development of the GEOS-5 atmospheric general circulation model: evolution from MERRA to MERRA2, *Geosci. Model Dev.*, 8, 1339–1356, doi:10.5194/gmd-8-1339-2015, 2015.
- 920 Morgenstern, O., Braesicke, P., O’Connor, F. M., Bushell, A. C., Johnson, C. E., Osprey, S. M., and Pyle, J. A.: Evaluation of the new UKCA climate-composition model – Part 1: The stratosphere, *Geosci. Model Dev.*, 2, 43–57, doi:10.5194/gmd-2-43- 2009, 2009.
- Morgenstern, O., Braesicke, P., O’Connor, F. M., Bushell, A. C., Johnson, C. E., Osprey, S. M., and Pyle, J. A.: Evaluation of the new UKCA climate-composition model – Part 1: The stratosphere, *Geosci. Model*
- 925 *Dev.*, 2, 43–57, doi:10.5194/gmd-2-43-2009, 2009.
- Morgenstern, O., Hegglin, M. I., Rozanov, E., amp, apos, Connor, F. M., Abraham, N. L., Akiyoshi, H., Archibald, A. T., Bekki, S., Butchart, N., Chipperfield, M. P., Deushi, M., Dhomse, S. S., Garcia, R. R., Hardiman, S. C., Horowitz, L. W., Jöckel, P., Josse, B., Kinnison, D., Lin, M., Mancini, E., Manyin, M. E., Marchand, M., Mar écal, V., Michou, M., Oman, L. D., Pitari, G., Plummer, D. A., Revell, L. E., Saint-
- 930 Martin, D., Schofield, R., Stenke, A., Stone, K., Sudo, K., Tanaka, T. Y., Tilmes, S., Yamashita, Y., Yoshida, K., and Zeng, G.: Review of the global models used within phase 1 of the Chemistry–Climate Model Initiative (CCMI), *Geoscientific Model Development*, 10, 639-671, doi:10.5194/gmd-10-639-2017, 2017.

- 935 Murray, L. T., Mickley, L. J., Kaplan, J. O., Sofen, E. D., Pfeiffer, M., and Alexander, B.: Factors
controlling variability in the oxidative capacity of the troposphere since the Last Glacial Maximum,
Atmos. Chem. Phys., 14, 3589-3622, doi:10.5194/acp-14-3589-2014, 2014.
- 940 Naik, V., Voulgarakis, A., Fiore, A. M., Horowitz, L. W., Lamarque, J. F., Lin, M., Prather, M. J., Young,
P. J., Bergmann, D., Cameron-Smith, P. J., Cionni, I., Collins, W. J., Dalsøren, S. B., Doherty, R., Eyring,
V., Faluvegi, G., Folberth, G. A., Josse, B., Lee, Y. H., MacKenzie, I. A., Nagashima, T., van Noije, T. P.
C., Plummer, D. A., Righi, M., Rumbold, S. T., Skeie, R., Shindell, D. T., Stevenson, D. S., Strode, S.,
945 Sudo, K., Szopa, S., and Zeng, G.: Preindustrial to present-day changes in tropospheric hydroxyl radical
and methane lifetime from the Atmospheric Chemistry and Climate Model Intercomparison Project
(ACCMIP), *Atmospheric Chemistry and Physics*, 13, 5277-5298, doi:10.5194/acp-13-5277-2013, 2013.
- 950 Neu, J. L., Prather, M. J., and Penner, J. E.: Global atmospheric chemistry: Integrating over fractional
cloud cover, *Journal of Geophysical Research: Atmospheres*, 112, D11306, doi:10.1029/2006JD008007,
2007.
- Nielsen, J. E., Pawson, S., Molod, A., Auer, B., da Silva, A. M., Douglass, A. R., Duncan, B., Liang, Q.,
Manyin, M., and Oman, L. D.: Chemical mechanisms and their applications in the Goddard Earth
Observing System (GEOS) earth system model, *Journal of advances in modeling earth systems*, 9, 3019-
955 3044, 2017.
- Nisbet, E. G., Manning, M. R., Dlugokencky, E. J., Fisher, R. E., Lowry, D., Michel, S. E., Myhre, C. L.,
Platt, S. M., Allen, G., Bousquet, P., Brownlow, R., Cain, M., France, J. L., Hermansen, O., Hossaini, R.,
Jones, A. E., Levin, I., Manning, A. C., Myhre, G., Pyle, J. A., Vaughn, B., Warwick, N. J., and White, J.
W. C.: Very strong atmospheric methane growth in the four years 2014-2017: Implications for the Paris
960 Agreement, *Global Biogeochemical Cycles*, 33, doi:10.1029/2018GB006009, 2019.
- O'Connor, F. M., Johnson, C. E., Morgenstern, O., Abraham, N. L., Braesicke, P., Dalvi, M., Folberth, G.
A., Sanderson, M. G., Telford, P. J., Voulgarakis, A., Young, P. J., Zeng, G., Collins, W. J., and Pyle, J. A.:
Evaluation of the new UKCA climatecomposition model – Part 2: The Troposphere, *Geosci. Model Dev.*,
7, 41–91, doi:10.5194/gmd-7-41-2014, 2014.
- 965 Oman, L. D., Ziemke, J. R., Douglass, A. R., Waugh, D. W., Lang, C., Rodriguez, J. M., and Nielsen, J.
E.: The response of tropical tropospheric ozone to ENSO, *Geophys. Res. Lett.*, 38, L13706,
doi:10.1029/2011GL047865, 2011.
- Oman, L. D., Douglass, A. R., Ziemke, J. R., Rodriguez, J. M., Waugh, D. W., and Nielsen, J. E.: The
ozone response to ENSO in Aura satellite measurements and a chemistry-climate simulation, *J. Geophys.*
970 *Res.*, 118, 965–976, doi:10.1029/2012JD018546, 2013.
- Patra, P. K., Houweling, S., Krol, M., Bousquet, P., Belikov, D., Bergmann, D., Bian, H., Cameron-Smith,
P., Chipperfield, M. P., Corbin, K., Fortems-Cheiney, A., Fraser, A., Gloor, E., Hess, P., Ito, A., Kawa, S.
R., Law, R. M., Loh, Z., Maksyutov, S., Meng, L., Palmer, P. I., Prinn, R. G., Rigby, M., Saito, R., and
Wilson, C.: TransCom model simulations of CH₄ and related species: linking transport, surface flux and
chemical loss with CH₄ variability in the troposphere and lower stratosphere, *Atmospheric Chemistry*

and Physics, 11, 12813-12837, doi:10.5194/acp-11-12813-2011, 2011.

Patra, P. K., Krol, M. C., Montzka, S. A., Arnold, T., Atlas, E. L., Lintner, B. R., Stephens, B. B., Xiang, B., Elkins, J. W., Fraser, P. J., Ghosh, A., Hints, E. J., Hurst, D. F., Ishijima, K., Krummel, P. B., Miller, B. R., Miyazaki, K., Moore, F. L., Mühle, J., O'Doherty, S., Prinn, R. G., Steele, L. P., Takigawa, M.,
975 Wang, H. J., Weiss, R. F., Wofsy, S. C., and Young, D.: Observational evidence for interhemispheric hydroxyl-radical parity, *Nature*, 513, doi:219, 10.1038/nature13721, 2014.

Pison, I., Bousquet, P., Chevallier, F., Szopa, S., and Hauglustaine, D.: Multi-species inversion of CH₄, CO and H₂ emissions from surface measurements, *Atmos. Chem. Phys.*, 9, 5281-5297, doi:10.5194/acp-9-5281-2009, 2009.

980 Poulter, B., Bousquet, P., Canadell, J. G., Ciais, P., Pregon, A., Saunois, M., Arora, V. K., Beerling, D. J., Brovkin, V., and Jones, C. D.: Global wetland contribution to 2000–2012 atmospheric methane growth rate dynamics, *Environmental Research Letters*, 12, 094013, 2017.

Prather, M. J., Holmes, C. D., and Hsu, J.: Reactive greenhouse gas scenarios: Systematic exploration of uncertainties and the role of atmospheric chemistry, *Geophysical Research Letters*, 39, L09803,
985 doi:10.1029/2012GL051440, 2012.

Price, C., and Rind, D.: Modeling Global Lightning Distributions in a General Circulation Model, *Monthly Weather Review*, 122, 1930-1939, doi:10.1175/1520-0493(1994)122<1930:mgldia>2.0.co;2, 1994.

Prinn, R. G., Huang, J., Weiss, R. F., Cunnold, D. M., Fraser, P. J., Simmonds, P. G., McCulloch, A., Harth, C., Reimann, S., Salameh, P., O'Doherty, S., Wang, R. H. J., Porter, L. W., Miller, B. R., and Krummel, P. B.: Evidence for variability of atmospheric hydroxyl radicals over the past quarter century, *Geophysical Research Letters*, 32, L07809, doi:10.1029/2004GL022228, 2005.

Randerson, J.T., G.R. van der Werf, L. Giglio, G.J. Collatz, and P.S. Kasibhatla. 2018. Global Fire Emissions Database, Version 4.1 (GFEDv4). ORNL DAAC, Oak Ridge, Tennessee, USA. doi:
995 <https://doi.org/10.3334/ORNLDAAC/1293>

Revell, L. E., Tummon, F., Stenke, A., Sukhodolov, T., Coulon, A., Rozanov, E., Garny, H., Grewe, V., and Peter, T.: Drivers of the tropospheric ozone budget throughout the 21st century under the medium-high climate scenario RCP 6.0, *Atmos. Chem. Phys.*, 15, 5887–5902, doi:10.5194/acp-15-5887-2015, 2015.

1000 Revell, L. E., Stenke, A., Tummon, F., Feinberg, A., Rozanov, E., Peter, T., Abraham, N. L., Akiyoshi, H., Archibald, A. T., Butchart, N., Deushi, M., Jöckel, P., Kinnison, D., Michou, M., Morgenstern, O., O'Connor, F. M., Oman, L. D., Pitari, G., Plummer, D. A., Schofield, R., Stone, K., Tilmes, S., Visioni, D., Yamashita, Y., and Zeng, G.: Tropospheric ozone in CCMi models and Gaussian process emulation to understand biases in the SOCOLv3 chemistry–climate model, *Atmos. Chem. Phys.*, 18, 16155-16172,
1005 doi:10.5194/acp-18-16155-2018, 2018.

Riahi, K., Rao, S., Krey, V., Cho, C., Chirkov, V., Fischer, G., Kindermann, G., Nakicenovic, N., and Rafaj, P.: RCP 8.5—A scenario of comparatively high greenhouse gas emissions, *Climatic Change*, 109,

33-57, 10.1007/s10584-011-0149-y, 2011.

Ridgwell, A. J., Marshall, S. J., and Gregson, K.: Consumption of atmospheric methane by soils: A process-based model, *Global Biogeochemical Cycles*, 13, 59-70, doi:10.1029/1998GB900004, 1999.

Rigby, M., Prinn, R. G., Fraser, P. J., Simmonds, P. G., Langenfelds, R. L., Huang, J., Cunnold, D. M., Steele, L. P., Krummel, P. B., Weiss, R. F., O'Doherty, S., Salameh, P. K., Wang, H. J., Harth, C. M., Mühle, J., and Porter, L. W.: Renewed growth of atmospheric methane, *Geophysical Research Letters*, 35, 10.1029/2008gl036037, 2008.

Rigby, M., Montzka, S. A., Prinn, R. G., White, J. W. C., Young, D., O'Doherty, S., Lunt, M. F., Ganesan, A. L., Manning, A. J., Simmonds, P. G., Salameh, P. K., Harth, C. M., Mühle, J., Weiss, R. F., Fraser, P. J., Steele, L. P., Krummel, P. B., McCulloch, A., and Park, S.: Role of atmospheric oxidation in recent methane growth, *Proc Natl Acad Sci U S A*, 114, 5373-5377, doi:10.1073/pnas.1616426114, 2017.

Sadourny, R., and Laval, K.: January and July performances of the LMD general circulation model, *New Perspectives in Climate Modeling*, In *New Perspectives in Climate Modeling*, A.L. Berger and C. Nicolis (eds.), Elsevier Press, Amsterdam, 173-197, 1984.

Sander, R., Jöckel, P., Kirner, O., Kunert, A. T., Landgraf, J., and Pozzer, A.: The photolysis module JVAL-14, compatible with the MESSy standard, and the JVal PreProcessor (JVPP), *Geosci. Model Dev.*, 7, 2653-2662, doi:10.5194/gmd-7-2653-2014, 2014.

Sander, S. P., Abbatt, J., Barker, J. R., Burkholder, J. B., Friedl, R. R., Golden, D. M., Huie, R., Kurylo, M. J., Moortgat, G. K., Orkin, V. L., and Wine, P. H.: Chemical kinetics and photochemical data for use in atmospheric studies evaluation number 17, Pasadena, CA: Jet Propulsion Laboratory, National Aeronautics and Space Administration, 2011.

Saunio, M., Bousquet, P., Poulter, B., Peregon, A., Ciais, P., Canadell, J. G., Dlugokencky, E. J., Etiope, G., Bastviken, D., Houweling, S., Janssens-Maenhout, G., Tubiello, F. N., Castaldi, S., Jackson, R. B., Alexe, M., Arora, V. K., Beerling, D. J., Bergamaschi, P., Blake, D. R., Brailsford, G., Brovkin, V., Bruhwiler, L., Crevoisier, C., Crill, P., Covey, K., Curry, C., Frankenberg, C., Gedney, N., Höglund-Isaksson, L., Ishizawa, M., Ito, A., Joos, F., Kim, H. S., Kleinen, T., Krummel, P., Lamarque, J. F., Langenfelds, R., Locatelli, R., Machida, T., Maksyutov, S., McDonald, K. C., Marshall, J., Melton, J. R., Morino, I., Naik, V., O'Doherty, S., Parmentier, F. J. W., Patra, P. K., Peng, C., Peng, S., Peters, G. P., Pison, I., Prigent, C., Prinn, R., Ramonet, M., Riley, W. J., Saito, M., Santini, M., Schroeder, R., Simpson, I. J., Spahni, R., Steele, P., Takizawa, A., Thornton, B. F., Tian, H., Tohjima, Y., Viovy, N., Voulgarakis, A., van Weele, M., van der Werf, G. R., Weiss, R., Wiedinmyer, C., Wilton, D. J., Wiltshire, A., Worthy, D., Wunch, D., Xu, X., Yoshida, Y., Zhang, B., Zhang, Z., and Zhu, Q.: The global methane budget 2000–2012, *Earth Syst. Sci. Data*, 8, 697-751, doi:10.5194/essd-8-697-2016, 2016.

Schultz, M. G., Heil, A., Hoelzemann, J. J., Spessa, A., Thonicke, K., Goldammer, J. G., Held, A. C., Pereira, J. M. C., and van het Bolscher, M.: Global wildland fire emissions from 1960 to 2000, *Global Biogeochemical Cycles*, 22, 10.1029/2007gb003031, 2008.

Scinocca, J. F., McFarlane, N. A., Lazare, M., Li, J., and Plummer, D.: Technical Note: The CCCma third

- 1045 generation AGCM and its extension into the middle atmosphere, *Atmos. Chem. Phys.*, 8, 7055–7074, doi:10.5194/acp-8-7055-2008, 2008.
- Sindelarova, K., Granier, C., Bouarar, I., Guenther, A., Tilmes, S., Stavrakou, T., Müller, J. F., Kuhn, U., Stefani, P., and Knorr, W.: Global data set of biogenic VOC emissions calculated by the MEGAN model over the last 30 years, *Atmospheric Chemistry and Physics*, 14, 9317-9341, doi:10.5194/acp-14-9317-2014, 2014.
- 1050 Solomon, S., Kinnison, D. E., Bandoro, J., and Garcia, R.: Simulations of polar ozone depletion: an update, *J. Geophys. Res.*, 120, 7958–7974, doi:doi:10.1002/2015JD023365, 2015.
- Spivakovsky, C. M., Logan, J. A., Montzka, S. A., Balkanski, Y. J., Foreman-Fowler, M., Jones, D. B. A., Horowitz, L. W., Fusco, A. C., Brenninkmeijer, C. A. M., Prather, M. J., Wofsy, S. C., and McElroy, M. B.: Three-dimensional climatological distribution of tropospheric OH: Update and evaluation, *Journal of Geophysical Research: Atmospheres*, 105, 8931-8980, doi:10.1029/1999jd901006, 2000.
- 1055 Stenke, A., Schraner, M., Rozanov, E., Egorova, T., Luo, B., and Peter, T.: The SOCOL version 3.0 chemistry-climate model: description, evaluation, and implications from an advanced transport algorithm, *Geosci. Model Dev.*, 6, 1407–1427, doi:10.5194/gmd-6-1407-2013, 2013.
- 1060 Staehelin, J., Tummon, F., Revell, L., Stenke, A., and Peter, T.: Tropospheric Ozone at Northern Mid-Latitudes: Modeled and Measured Long-Term Changes, *Atmosphere*, 8, 163, 2017.
- Stohl, A., Aamaas, B., Amann, M., Baker, L. H., Bellouin, N., Berntsen, T. K., Boucher, O., Cherian, R., Collins, W., Daskalakis, N., Dusinska, M., Eckhardt, S., Fuglestedt, J. S., Harju, M., Heyes, C., Hodnebrog, Ø., Hao, J., Im, U., Kanakidou, M., Klimont, Z., Kupiainen, K., Law, K. S., Lund, M. T., 1065 Maas, R., MacIntosh, C. R., Myhre, G., Myriokefalitakis, S., Olivi é D., Quaas, J., Quennehen, B., Raut, J. C., Rumbold, S. T., Samset, B. H., Schulz, M., Seland, Ø., Shine, K. P., Skeie, R. B., Wang, S., Yttri, K. E., and Zhu, T.: Evaluating the climate and air quality impacts of short-lived pollutants, *Atmos. Chem. Phys.*, 15, 10529-10566, doi: 10.5194/acp-15-10529-2015, 2015.
- Strode, S. A., Duncan, B. N., Yegorova, E. A., Kouatchou, J., Ziemke, J. R., and Douglass, A. R.: 1070 Implications of carbon monoxide bias for methane lifetime and atmospheric composition in chemistry climate models, *Atmos. Chem. Phys.*, 15, 11789-11805, doi: 10.5194/acp-15-11789-2015, 2015.
- Strode SA et al. (2016) Interpreting space-based trends in carbon monoxide with multiple models *Atmos Chem Phys* 16:7285-7294 doi:10.5194/acp-16-7285-2016
- Sukhodolov, T., Rozanov, E., Ball, W.T., Bais, A., Tourpali, K., Shapiro, A.I., Telford, P., Smyshlyaev, S., 1075 Fomin, B., Sander, R., Bossay, S., Bekki, S., Marchand, M., Chipperfield, M.P., Dhomse, S., Haigh, J.D., Peter, T., Schmutz, W., 2016. Evaluation of simulated photolysis rates and their response to solar irradiance variability. *Journal of Geophysical Research: Atmospheres* 121, 6066-6084.
- Szopa, S., Balkanski, Y., Schulz, M., Bekki, S., Cugnet, D., Fortems-Cheiney, A., Turquety, S., Cozic, A., D éandreis, C., Hauglustaine, D., Idelkadi, A., Lathi ère, J., Lefevre, F., Marchand, M., Vuolo, R., Yan, N., 1080 and Dufresne, J.-L.: Aerosol and ozone changes as forcing for climate evolution between 1850 and 2100, *Climate Dynamics*, 40, 2223-2250, doi:10.1007/s00382-012-1408-y, 2013.

Telford, P. J., Abraham, N. L., Archibald, A. T., Braesicke, P., Dalvi, M., Morgenstern, O., O'Connor, F. M., Richards, N. A. D., and Pyle, J. A.: Implementation of the Fast-JX Photolysis scheme (v6.4) into the UKCA component of the MetUM chemistry-climate model (v7.3), *Geosci. Model Dev.*, 6, 161-177, doi:10.5194/gmd-6-161-2013, 2013.

Terrenoire, E., D. A. Hauglustaine, R. Valorso, and A. Cozic, Impact of present and future aircraft NO_x and aerosol emissions on atmospheric composition and radiative forcing of climate, *Atmos. Chem. Phys.* in preparation, 2019.

Teyss re, H., Michou, M., Clark, H. L., Josse, B., Karcher, F., Olivi  D., Peuch, V. H., Saint-Martin, D., Cariolle, D., Atti  J. L., N d ec, P., Ricaud, P., Thouret, V., van der A, R. J., Volz-Thomas, A., and Ch roux, F.: A new tropospheric and stratospheric Chemistry and Transport Model MOCAGE-Climat for multi-year studies: evaluation of the present-day climatology and sensitivity to surface processes, *Atmos. Chem. Phys.*, 7, 5815-5860, doi:10.5194/acp-7-5815-2007, 2007.

Tilmes, S., Lamarque, J.-F., Emmons, L. K., Kinnison, D. E., Ma, P.-L., Liu, X., Ghan, S., Bardeen, C., Arnold, S., Deeter, M., Vitt, F., Ryerson, T., Elkins, J.W., Moore, F., Spackman, J. R., and Val Martin, M.: Description and evaluation of tropospheric chemistry and aerosols in the Community Earth System Model (CESM1.2), *Geosci. Model Dev.*, 8, 1395-1426, doi:10.5194/gmd-8-1395-2015, 2015.

Tilmes, S., Lamarque, J.-F., Emmons, L. K., Kinnison, D. E., Marsh, D., Garcia, R. R., Smith, A. K., Neely, R. R., Conley, A., Vitt, F., Val Martin, M., Tanimoto, H., Simpson, I., Blake, D. R., and Blake, N.: Representation of the Community Earth System Model (CESM1) CAM4-chem within the Chemistry-Climate Model Initiative (CCMI), *Geosci. Model Dev.*, 9, 1853-1890, doi: <https://doi.org/10.5194/gmd-9-1853-2016>, 2016.

Turner, A. J., Frankenberg, C., Wennberg, P. O., and Jacob, D. J.: Ambiguity in the causes for decadal trends in atmospheric methane and hydroxyl, *Proc Natl Acad Sci U S A*, 114, 5367-5372, doi:10.1073/pnas.1616020114, 2017.

van der Werf, G. R., Randerson, J. T., Giglio, L., Collatz, G. J., Kasibhatla, P. S., and Arellano Jr, A. F.: Interannual variability in global biomass burning emissions from 1997 to 2004, *Atmos. Chem. Phys.*, 6, 3423-3441, 10.5194/acp-6-3423-2006, 2006.

Vinken, G. C. M., Boersma, K. F., Maasakkers, J. D., Adon, M., and Martin, R. V.: Worldwide biogenic soil NO_x emissions inferred from OMI NO₂ observations, *Atmos. Chem. Phys.*, 14, 10363-10381, doi: 10.5194/acp-14-10363-2014, 2014.

Voulgarakis, A., Naik, V., Lamarque, J. F., Shindell, D. T., Young, P. J., Prather, M. J., Wild, O., Field, R. D., Bergmann, D., Cameron-Smith, P., Cionni, I., Collins, W. J., Dals ren, S. B., Doherty, R. M., Eyring, V., Faluvegi, G., Folberth, G. A., Horowitz, L. W., Josse, B., MacKenzie, I. A., Nagashima, T., Plummer, D. A., Righi, M., Rumbold, S. T., Stevenson, D. S., Strode, S. A., Sudo, K., Szopa, S., and Zeng, G.: Analysis of present day and future OH and methane lifetime in the ACCMIP simulations, *Atmospheric Chemistry and Physics*, 13, 2563-2587, 10.5194/acp-13-2563-2013, 2013.

Wang, Y., and Jacob, D. J.: Anthropogenic forcing on tropospheric ozone and OH since preindustrial

times, *Journal of Geophysical Research: Atmospheres*, 103, 31123-31135, doi:10.1029/1998JD100004, 1998.

Yienger, J. J., and Levy, H.: Empirical model of global soil-biogenic NO_x emissions, *Journal of Geophysical Research: Atmospheres*, 100, 11447-11464, doi:10.1029/95JD00370, 1995.

Yukimoto, S., Yoshimura, H., Hosaka, M., Sakami, T., Tsujino, H., Hirabara, M., Tanaka, T. Y., Deushi, M., Obata, A., Nakano, H., Adachi, Y., Shindo, E., Yabu, S., Ose, T., and Kitoh, A.: Meteorological Research Institute Earth System Model Version 1 (MRIESM1).

van der Werf, G. R., Randerson, J. T., Giglio, L., Collatz, G. J., Mu, M., Kasibhatla, P. S., Morton, D. C., DeFries, R. S., Jin, Y., and van Leeuwen, T. T.: Global fire emissions and the contribution of deforestation, savanna, forest, agricultural, and peat fires (1997–2009), *Atmos. Chem. Phys.*, 10, 11707-11735, 10.5194/acp-10-11707-2010, 2010.

Walters, D. N., Williams, K. D., Boutle, I. A., Bushell, A. C., Edwards, J. M., Field, P. R., Lock, A. P., Morcrette, C. J., Stratton, R. A., Wilkinson, J. M., Willett, M. R., Bellouin, N., Bodas-Salcedo, A., Brooks, M. E., Copestake, D., Earnshaw, P. D., Hardiman, S. C., Harris, C. M., Levine, R. C., MacLachlan, C., Manners, J. C., Martin, G. M., Milton, S. F., Palmer, M. D., Roberts, M. J., Rodriguez, J. M., Tennant, W. J., and Vidale, P. L.: The Met Office Unified Model Global Atmosphere 4.0 and JULES Global Land 4.0 configurations, *Geosci. Model Dev.*, 7, 361–386, doi:10.5194/gmd-7-361-2014, 2014.

World Meteorological Organization: Definition of the tropopause, *Bulletin of the World Meteorological Organization*, 6, 136–137, 1957.

Zimmerman, P. R., Chatfield, R. B., Fishman, J., Crutzen, P. J., and Hanst, P. L.: Estimates on the production of CO and H₂ from the oxidation of hydrocarbon emissions from vegetation, *Geophysical Research Letters*, 5, 679-682, doi:10.1029/GL005i008p00679, 1978.

Zimmermann, P. H., Brenninkmeijer, C. A. M., Pozzer, A., Jöckel, P., Zahn, A., Houweling, S., and Lelieveld, J.: Model simulations of atmospheric methane and their evaluation using AGAGE/NOAA surface- and IAGOS-CARIBIC aircraft observations, 1997–2014, *Atmospheric Chemistry and Physics Discussions*, doi: 1-45, 10.5194/acp-2017-1212, 2018.

Tables

1160

Table 1. List of CCMI models included in this study with model versions and references.¹

Model	Version	References
CESM1-CAM-chem	CCMI_23	Tilmes et al.(2015, 2016)
CESM1-WACCM	CCMI_30	Solomon et al. (2015); Garcia et al. (2016); Marsh et al. (2013)
CMAM	v2.1	Jonsson et al. (2004); Scinocca et al. (2008)
EMAC(offering two resolutions: EMAC-L47MA and EMAC-L90MA)	v2.51	Jöckel et al. (2010, 2016)
GEOSCCM	v3	Molod et al. (2012, 2015); Oman et al. (2011, 2013); Nielsen et al. (2017)
HadGEM3-ES	HadGEM3 GA4.0, NEMO 3.4, CICE, UKCA, MetUM8.2	Walters et al.(2014); Madec(2008); Hunke and Lipscombe(2008); Morgenstern et al.(2009); O'Connor et al.(2004); Hardiman et al.(2017)
MOCAGE	v2.15.1	Josse et al. (2004); Guth et al. (2016)
MRI-ESM1r1	v1.1	Yukimoto et al. (2012, 2011); Deushi and Shibata (2011)
SOCOL3	v3	Revell et al. (2015); Stenke et al. (2013)
UMUKCA-UCAM	MetUM 7.3	Morgenstern et al. (2009); Bednarz et al. (2016)

¹ The table refers to Table 2 in Morgenstern et al. (2017)

Table 2. List of LMDz experiments and model setups.

	Simulation period	Inter annual variability in [OH]	Inter annual variability in CH ₄ emissions
Run_standard	2000-2010	2000-2010	2000-2010
Run_REF-C2	2011-2016	2010 apply inter-annual variability from REF-C2	2011-2016
Run_OH_inc	2011-2016	2010 apply annual growth rate of 1%	2011-2016

Run_OH_dec	2011-2016	2010 apply annual decrease rate of 1%	2011-2016
Run_fix_OH	2000-2016	Constant OH (year 2000)	2010-2016
Run_fix_emis	2000-2010	2000-2010(CESM-WACCM only)	Constant (2000)
Run_fix_emis_oh	2000-2010	Constant OH (year 2000 CESM-WACCM only)	Constant (2000)

1165

Table 3. Inter-hemispheric ratios (N/S) of hemispheric mean OH and volume-weighted tropospheric mean [OH] for four latitude bands (in 10^5 molec.cm⁻³) averaged over the years 2000 to 2010. Multi-model means and standard deviations (Mean \pm stand. dev.) are also shown.

1170

OH fields	N/S ratio	90°S-30°S (10^5 molec.cm ⁻³)	30°S-0° (10^5 molec.cm ⁻³)	0°-30°N (10^5 molec.cm ⁻³)	30°N-90°N (10^5 molec.cm ⁻³)
TransCom	1.0	5.8	12.7	11.8	6.2
INCA NMHC-AER-S	1.3	4.7	10.6	12	7.5
INCA NMHC	1.2	5.7	11.9	13.4	7.8
CESM1-CAM4Chem	1.4	5.7	12.4	15.3	9.2
CESM1-WACCM	1.3	5.9	12.3	15.1	9.3
CMAM	1.2	5.6	13.1	14.3	8.3
EMAC-L47MA	1.2	6	13.5	15.6	8.4
EMAC-L90MA	1.2	6.3	13.8	15.7	8.6
GEOSCCM	1.2	6.5	14.8	16.8	9.1
HadGEM3-ES	1.4	4.1	10.4	12.5	8.1
MOCAGE	1.5	5.5	11.4	14.3	10.2
MRI-ESM1r1	1.2	4.7	13.7	15.3	7.3
SOCOL3	1.5	6.8	13.5	17.0	14.0
UMUKCA-UCAM	1.3	5.6	13.7	14.9	9.9
Mean \pm stand. dev.	1.3 \pm 0.1	5.6 \pm 0.7	12.7 \pm 1.3	14.6 \pm 1.6	8.9 \pm 1.8

Table 4. Global mean [OH] averaged over the troposphere and three vertical pressure levels (in 10^5 molec cm⁻³) over the years 2000 to 2010. Multi-model means and standard deviations (Mean \pm stand. dev.) are also shown.

1175

	Tp-v ¹	Tp-m ²	750 ³	500	250	Tp scaled ⁴	CH ₄ lifetime ⁵
TransCom	9.1	10.0	9.9	12.8	9.2	9.5	/

INCA NMHC-AER-S	8.7	9.4	11.3	10.4	7.8	9.3	/
INCA NMHC	9.7	10.4	11.8	11.4	8.9	9.7	/
CESM1-CAM4Chem	10.7	11.3	12.2	12.3	10.7	/	9.4 yr
CESM1-WACCM	10.7	11.4	12.4	12.5	10.7	9.9	9.3 yr
CMAM	10.4	11.3	14.3	11	10.5	9.3	9.0 yr
EMAC-L47MA	10.9	11.3	12.1	12	10.3	/	/
EMAC-L90MA	11.1	11.5	12.5	12.2	10.2	10.3	/
GEOSCCM	11.8	12.3	12.3	13.7	12	10.4	8.9 yr
HadGEM3-ES	8.8	9.9	12.7	10.8	7.7	/	/
MOCAGE	10.4	12.5	19	13.5	7.7	7.7	7.5 yr
MRI-ESM1r1	10.3	10.6	12.2	10.4	9.4	10.2	10.0 yr
SOCOL3	12.8	14.4	19.4	15.1	10.9	9.0	7.1 yr
UMUKCA-UCAM	11.0	11.9	14.9	11.7	10.5	/	/
Mean \pm stand. Dev.	10.5 \pm 1.1	11.3 \pm 1.3	13.4 \pm 2.7	12.1 \pm 1.3	9.8 \pm 1.3	9.5 \pm 0.8	8.7 \pm 1.1 yr

¹ Tp-v refers to the volume-weighted tropospheric mean [OH].

² Tp-m refers to the mass-weighted tropospheric mean [OH]

³ 750 refers to the volume-weighted average from the surface to 750hPa, 500 refers to the volume-weighted average from 750hPa to 500 hPa, and 250 refers to the volume-weighted average from 500 to 250hPa.

⁴ Tp scaled refer to the volume-weighted global tropospheric mean [OH] after scaling to the same CH₄ loss as with INCA NMHC in 2000.

⁵ CH₄ lifetime is calculated global atmospheric CH₄ burden divided by annual total CH₄ tropospheric chemical loss.

Table 5. Global volume-weighted mean CO, N, and O₃ mixing ratios averaged over the whole troposphere and three pressure altitude levels for CCM1 models over 2000 to 2010.¹ Multi-model means and standard deviations (Mean \pm stand. dev.) are also shown.

	CO ppbv				NO pptv				O ₃ ppbv			
	750	500	250	Tp	750	500	250	Tp	750	500	250	Tp
CESM1-CAM4Chem	76	71	70	71	9	4	12	13	32	42	57	48
CESM1-WACCM	75	70	69	70	9	5	12	12	31	41	55	47
CMAM	77	68	64	69	17	4	17	26	34	43	60	52
EMAC-L47MA	85	77	70	75	8	4	11	14	38	48	63	56
EMAC-L90MA	84	76	69	74	8	5	11	17	38	48	61	54
GEOSCCM	78	74	73	74	9	5	13	13	33	43	61	49
MOCAGE	67	68	67	67	26	14	17	20	37	42	46	43
MRI-ESM1r1	93	86	83	86	10	5	20	32	36	48	67	56

SOCOL3	79	73	74	74	48	10	14	25	43	54	67	61
Mean ±stand. dev.	79±7	74±6	71±5	73±5	16±13	6±3	14±3	19±7	36±4	45±5	60±7	52±6

1190

¹ HadGEM3-ES and UMUKCA-UCAM are not analyzed since model output has been regridded to too coarse vertical pressure levels.

² Tp refers to the total tropospheric average, 750 refers to the average from the surface to 750hPa, 500 refers to the average from 750hPa to 500hPa, and 250 refers to the average from 500hPa to 250hPa.

1195

Table 6. Global mean tropospheric CH₄ mixing ratios as simulated by LMDz using different OH fields and repeating year 2000 over 30 times.

CH ₄ mixing ratio (ppbv)			
INCA NMHC-AER-S	1822	CESM1-WACCM	1575
TransCom	1776	CMAM	1540
INCA NMHC	1709	GEOSCCM	1503
MRI-ESM1r1	1693	MOCAGE	1275
EMAC-L90MA	1579	SOCOL3	1204

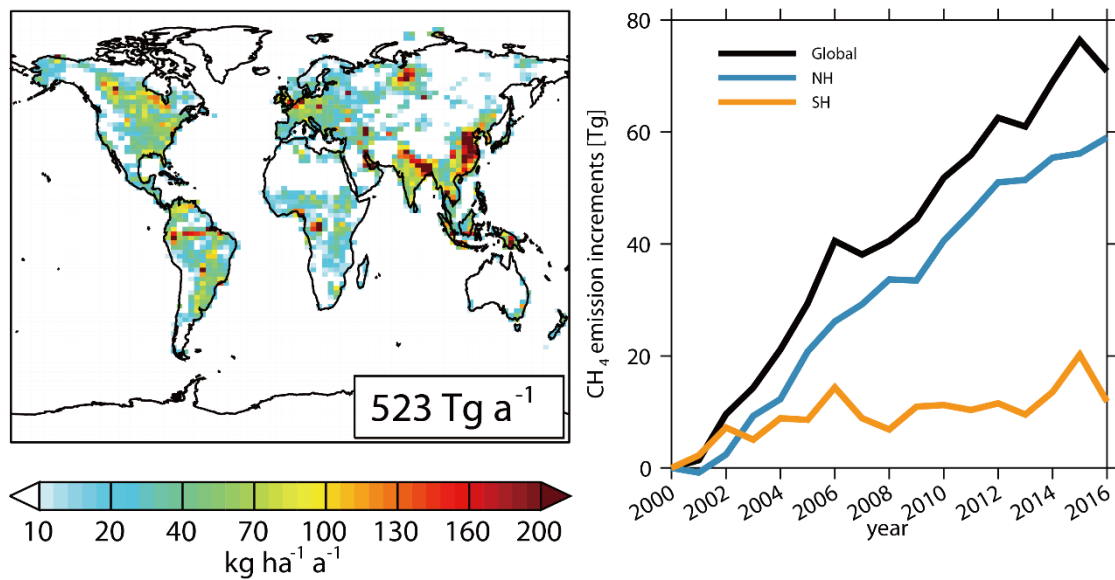
1200

Table 7. LMDz simulated CH₄ mixing ratios (in ppbv) averaged over each latitudinal band and the years 2000 to 2010 simulated from the standard experiment (Run_standard) using different OH fields. Multi-model means and standard deviations (Mean ±stand. dev.) are also shown.

	90 °S-60 °S	60 °S-0 °	0 °-60 °N	60 °N-90 °N	N/S gradient ¹
TransCom	1683	1697	1769	1812	129
INCA NMHC-AER-S	1687	1698	1757	1795	108
INCA NMHC	1687	1700	1762	1802	115
CESM1-WACCM	1688	1701	1757	1794	106
CMAM	1682	1694	1756	1796	114
EMAC-L90MA	1685	1698	1759	1798	113
GEOSCCM	1688	1701	1764	1803	115
MOCAGE	1686	1699	1753	1788	102
MRI-ESM1r1	1691	1702	1762	1803	112
SOCOL3	1694	1707	1754	1784	90
Mean ±stand. dev.	1687±4	1700±3	1759±5	1798±8	110±10

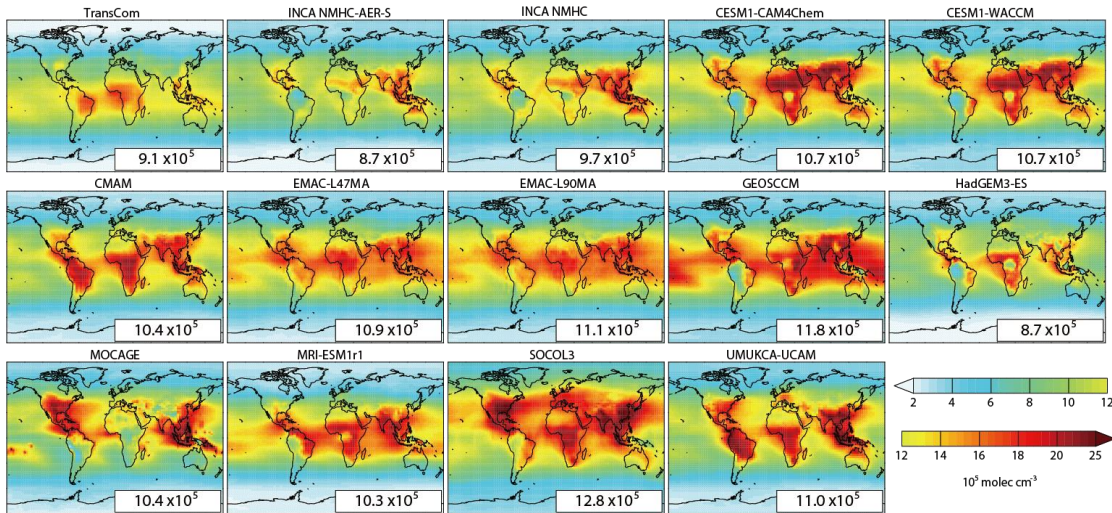
¹ N/S gradient is defined as the difference between 60 °N to 90 °N and 60 °S to 90 °S.

Figures



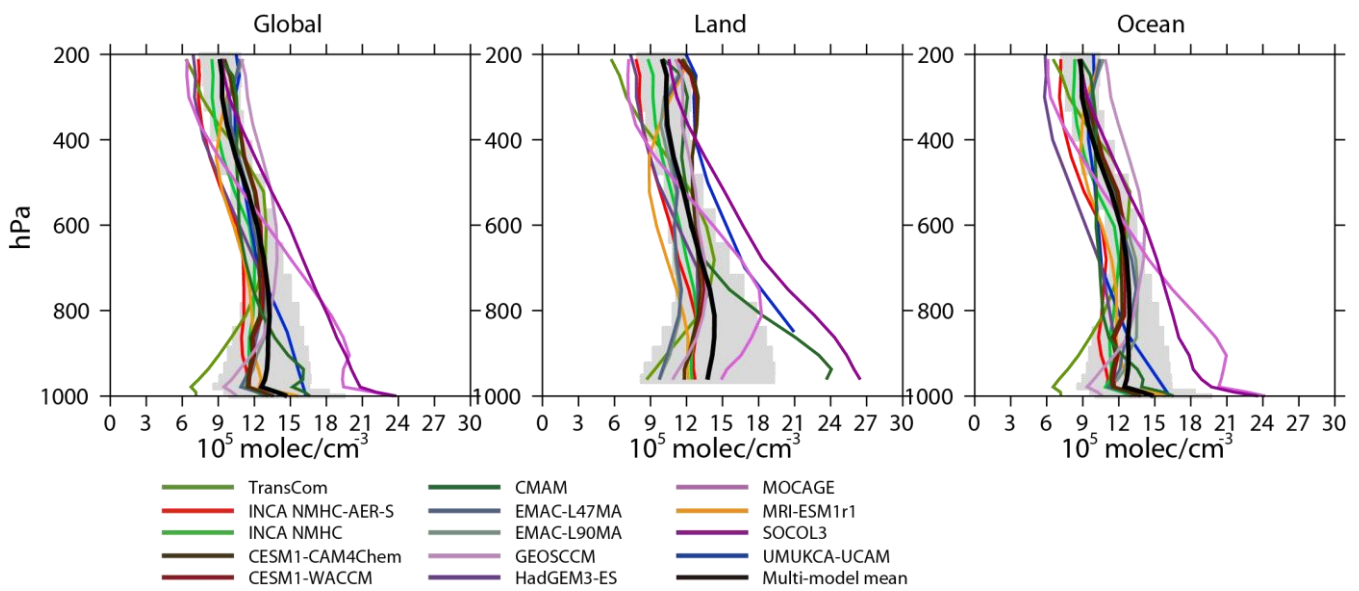
1210

Figure 1. Spatial distribution of global CH₄ emissions averaged between 2000 and 2016 (left) and a time series of CH₄ emissions relative to year 2000 emissions (482 Tg CH₄ a⁻¹) (right) for the globe (black line), Northern hemisphere (NH, blue line) and Southern hemisphere (SH, yellow line), respectively.



1215

Figure 2. The spatial distributions of volume-weighted tropospheric mean OH fields of TransCom, INCA, and CCMI models averaged for 2000-2010. Global mean values ($10^5 \text{ molec cm}^{-3}$) are shown as insets.



1220

Figure 3. Vertical distributions of [OH] averaged over the globe (left), land (middle) and ocean (right) for 2000-2010. Color lines represent [OH] from individual model simulations, black lines represent multi-model mean values and grey shades represent the standard deviations.

1225

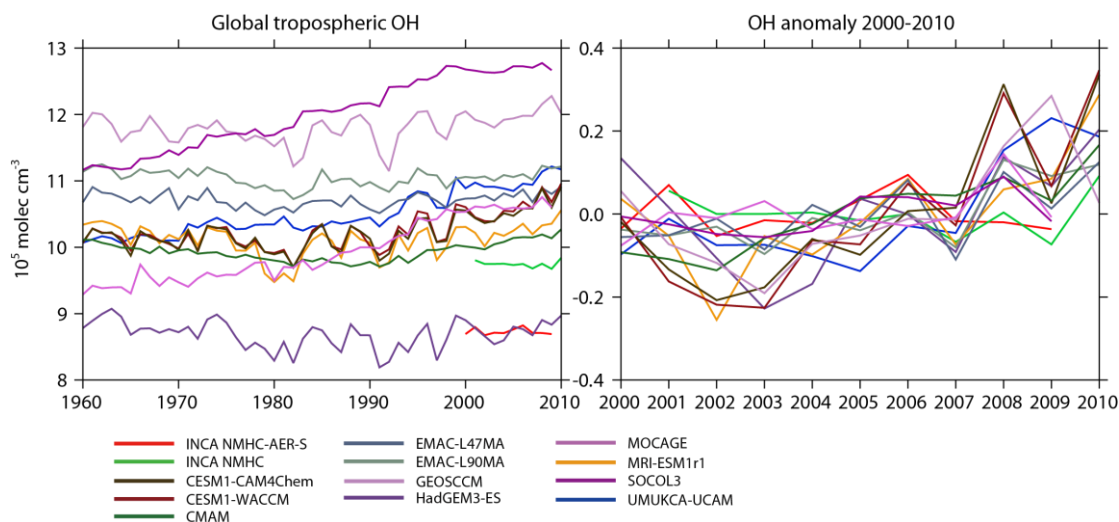


Figure 4. Left: Inter-annual variations of global volume-weighted tropospheric mean [OH] from CCMI and INCA model simulations from 1960 to 2010. Right: OH anomaly during 2000-2010, in reference to the mean concentration over the period 2000-2010 for each model.

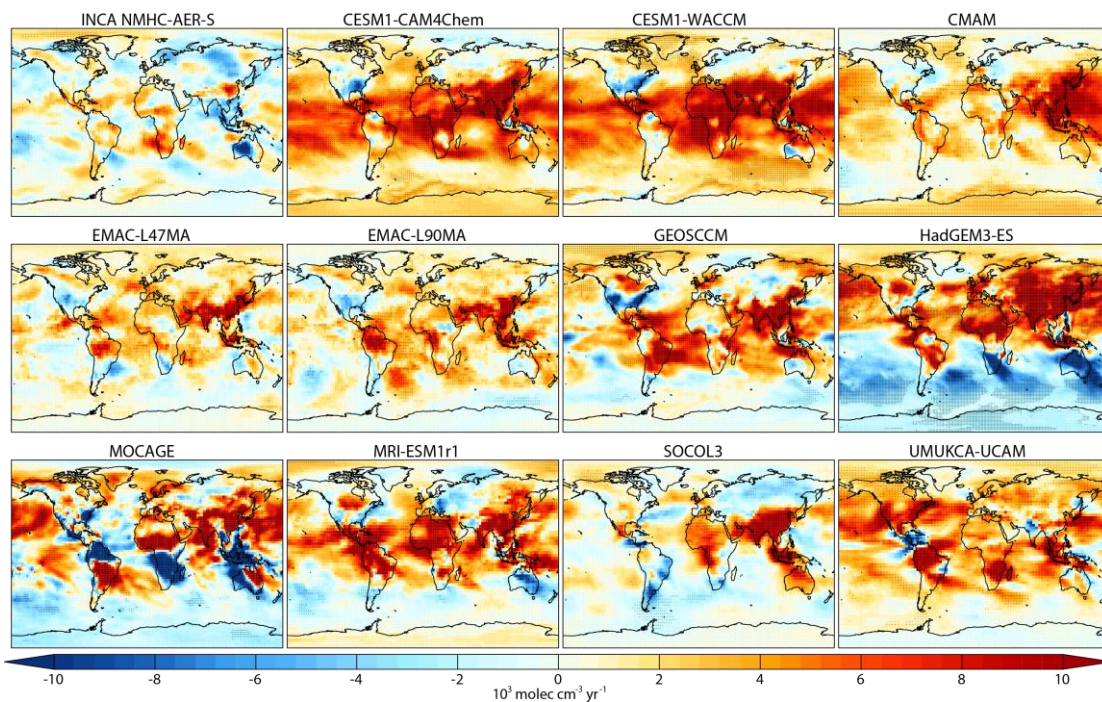


Figure 5. Spatial distribution of tropospheric OH trends from 2000 to 2010 (in $10^3 \text{ molec cm}^{-3} \text{ yr}^{-1}$). Black dots denote model grid-cells with statistically significant trends (p -value < 0.05)

1230

1235

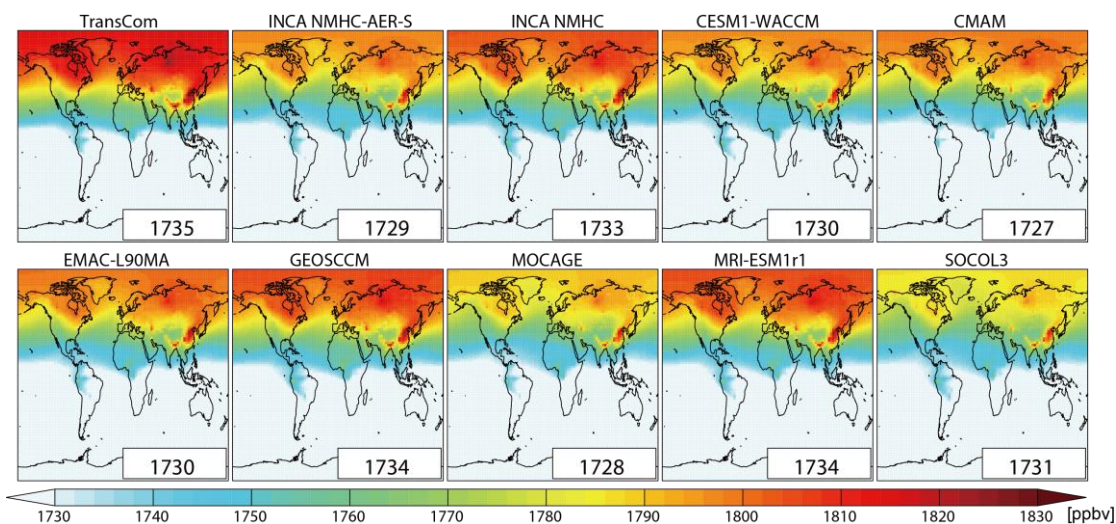


Figure 6. Spatial distribution of volume-weighted tropospheric mean CH_4 mixing ratios averaged from 2000 to 2010 as simulated by LMDz with different OH fields in the LMDz model. The global mean values in units of ppbv are shown as insets.

1240

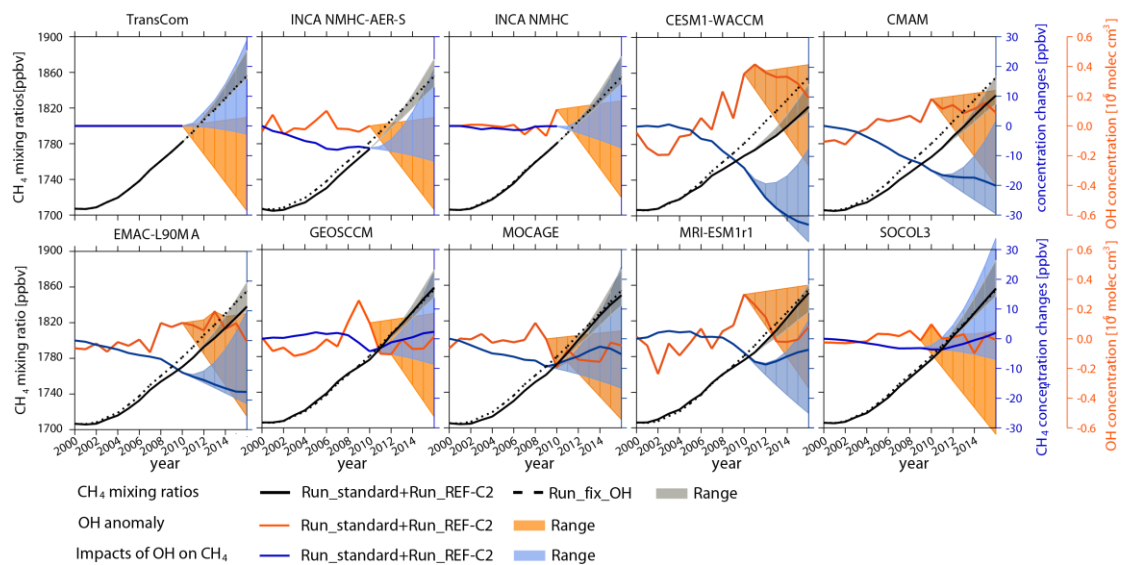


Figure 7. Time-series of global tropospheric CH_4 mixing ratios and $[\text{OH}]$ associated with the model experiments listed in Table 2. The black lines represent the evolution of CH_4 mixing ratios with varying (solid lines) or with constant (dashed lines) OH. The varying OH case is obtained using OH inputs from Run_standard from 2000 to 2010 followed by Run_REF-C2 from 2011 to 2016 (see Table 2). The blue solid lines represent the corresponding differences between the simulations with varying OH and with constant OH. The orange solid line represents the corresponding anomalies in tropospheric $[\text{OH}]$ (with

1245

the average over 2000-2010 as reference). The shaded areas correspond to the range obtained from all simulations over 2010-2016 (Table 2) for tropospheric CH₄ mixing ratios (grey), for changes in tropospheric CH₄ mixing ratios (blue) and for changes in tropospheric [OH] (orange).

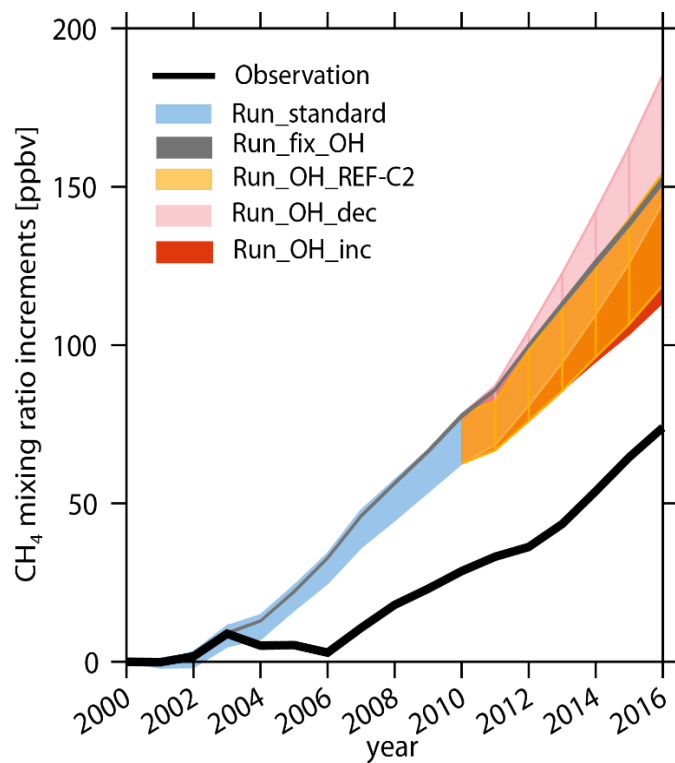


Figure 8. Time series of surface CH₄ mixing ratio increments compared to 2000 for NOAA observations (black line) and model ranges from all the LMDz experiments collected at observation sites (shades) and described in the text and in Table 2.

